TECHNISCHE UNIVERSITÄT WIEN

D I P L O M A R B E I T

Classification of Late-Antique Glass: Tandem-LIBS-LA-ICP-MS Analysis and Machine Learning Approach

by Barbara Umfahrer, BSc

carried out to obtain the degree Master of Science (MSc), submitted at TU Wien, Faculty of Technical Chemistry

under the supervision of

Univ.Prof. Dipl.-Ing. Dr. techn. Andreas Limbeck

and Projektass. Dipl.-Ing. Dr. techn. Lukas Brunnbauer, BSc

Institute of Chemical Technologies and Analytics

date, signature of the student

Abstract

Elemental analysis of a material reveals its characteristic chemical fingerprint, aiding in identifying the provenance of the raw materials and providing insights into historical trading routes. In the field of Archaeological Science, Laser Ablation-Inductively Coupled Plasma-Mass Spectrometry (LA-ICP-MS) is commonly used to analyze historical glass. This work aims to explore the advantages of incorporating Laser-Induced Breakdown Spectroscopy (LIBS) into the measurement setup, using Tandem-LIBS-LA-ICP-MS. The primary goal of this thesis is to develop a measurement methodology using the Tandem-LIBS-LA-ICP-MS configuration to generate high-quality data. This data will, in turn, be employed for the classification of the provided glass samples, utilizing a reference dataset that contains elemental analysis data derived from late-antique glasses as documented in existing literature.

Overall 46 late-antique glass samples, excavated at Hemmaberg, Austria, were analyzed and quantified using Tandem-LIBS-LA-ICP-MS and the reference materials NIST® SRM® 610 and NIST® SRM® 612. Solid measurements were validated against acid-digested samples, measured using conventional liquid ICP-OES and -MS. Moreover, a OneClass Support Vector Machine (OCSVM) was employed to determine novel glass types within the analyzed samples. Also, a k-nearest neighbor (k-NN)-model was trained to determine the provenance and assign the samples to glass types documented in the literature.

Solid measurements in general are minimal-invasive and sample preparation is less laborious. When it comes to quantification, the sum normalization method improved the results for two key elements when employing LIBS. This, in turn, enables the liberation of acquisition time in LA-ICP-MS, allowing for more precise measurements of other elements. Novelties could be detected and successful classification using k-NN was achieved using the samples' base compositions, assessable through LIBS data exclusively. The use of Recycling Markers, measured via LA-ICP-MS, allowed for the identification of recycled glass.

In the future, through the selection of more suitable reference materials and refining trace marker identification for sensitive LIBS measurements, it becomes feasible to eliminate the necessity of LA-ICP-MS within in the measurement setup. Such advancements could lead to LIBS-only measurements, potentially enabling handheld applications, greatly benefiting archaeologists in the field for rapid and on-site glass analysis.

Kurzfassung

Die Elementaranalyse eines Materials offenbart seinen charakteristischen chemischen Fingerabdruck. In der Archäometrie kann dieser dazu beitragen, die Herkunft der verwendeten Rohstoffe zu bestimmen und in Folge Einblicke in historische Handelswege zu gewinnen. Hierfür wird zur Analyse von historischem Glas üblicherweise die „Laser Ablation-Inductively Coupled Plasma-Mass Spectrometry“ (LA-ICP-MS) eingesetzt. In dieser Arbeit sollen die Vorteile der Einbeziehung der „Laser-Induced Breakdown Spectroscopy“ (LIBS) in den Messaufbau, unter Verwendung von Tandem-LIBS-LA-ICP-MS, untersucht werden. Es ist das Ziel, eine Messmethode zur Quantifizierung der Glasproben mit Tandem-LIBS-LA-ICP-MS zu entwickeln. Auf Grund der gewonnenen Messergebnisse und eines Referenzdatensatzes, der Elementanalysedaten von spätantiken Gläsern beinhaltet, die in der verfügbaren Literatur verzeichnet sind, sollen die Glasproben klassifiziert werden.

Es wurden 46 spätantike Glasproben, die am Hemmaberg, Österreich, ausgegraben wurden, mittels Tandem-LIBS-LA-ICP-MS und den Referenzmaterialien NIST® SRM® 610 und NIST® SRM® 612 analysiert und quantifiziert. Die Feststoffmessungen wurden anhand von mit Säure aufgeschlossenen Proben validiert, die mit herkömmlicher Flüssig-ICP-OES und -MS gemessen wurden. Darüber hinaus wurde eine OneClass Support Vector Machine (OCSVM) trainiert, um neue Glastypen innerhalb der analysierten Proben zu bestimmen. Außerdem wurden k-nearest neighbor-Modelle (k-NN) eingesetzt, um die Herkunft zu bestimmen und die Proben den in der Literatur dokumentierten Glastypen zuzuordnen.

Generell sind Festkörpermessungen im Vergleich zu Flüssigmessungen minimalinvasiv und die Probenvorbereitung ist weniger aufwändig. Hinsichtlich der Quantifizierung verbesserte die Einbeziehung der Methode der „sum normalization“ die Ergebnisse für zwei Schlüsselelemente bei der Verwendung von LIBS. Die Auswertung spezifischer Elemente mittels LIBS ermöglicht es, die Messzeit der LA-ICP-MS zu erweitern, was wiederum eine genauere Analyse weiterer Komponenten ermöglicht. Gläser, die sich auf Grund ihrer Grundzusammensetzung, die alleine durch LIBS bestimmt werden konnte, von jenen Gläsern im Referenzdatensatz unterscheiden, konnten erkannt und eine erfolgreiche Klassifizierung mit k-NN erreicht werden. Die Verwendung von Recycling-Markern, die mittels LA-ICP-MS gemessen wurden, ermöglichte die Identifizierung von recyceltem Glas.

Die mögliche Eliminierung von LA-ICP-MS aus dem Messaufbau könnte in Zukunft durch die Auswahl besser geeigneter Referenzmaterialien und die Verfeinerung der Auswahl von Spurenmarkern für empfindlichere LIBS-Messungen erreicht werden. Solche Fortschritte könnten zu reinen LIBS-Messungen führen, die eventuell tragbare Anwendungen

ermöglichen, was für Archäologinnen und Archäologen von großem Nutzen wäre, um Glas schnell und vor Ort zu analysieren.

Danksagung

Ich möchte gerne diese Gelegenheit nutzen, um meinen aufrichtigen Dank an all jene Personen auszusprechen, die einen entscheidenden Beitrag zur Entstehung dieser Arbeit geleistet haben.

Vor allem möchte ich Andreas Limbeck meine Dankbarkeit aussprechen. Er hat mich nicht nur bei der Themenfindung unterstützt, sondern mir überhaupt erst die Möglichkeit gegeben, Teil dieses Forschungsteams zu werden. Seine großartige Arbeitsgruppe hat mich herzlich aufgenommen, eine angenehme Arbeitsatmosphäre geschaffen und immerzu Hilfestellungen geboten.

Ein besonderer Dank gebührt meinem Mitbetreuer Lukas Brunnbauer, der mich von Anfang an ermutigt hat, neues Wissen zu erlangen, mich selbst zu fordern und an mich und mein Können zu glauben. Sein konstantes Feedback und seine aktive Beteiligung an meinen Gedanken und Zwischenergebnissen waren von unschätzbarem Wert für den Erfolg dieser Arbeit.

Ebenso möchte ich Pamela Fragnoli und Sabine Ladstätter vom Österreichischen Archäologischen Institut (ÖAI) für ihre Unterstützung danken. Schon an meinem ersten Arbeitstag als studentische Mitarbeiterin am ÖAI inspirierten sie mich dazu, eine Masterarbeit mit archäologischem Material zu verfassen, und Pamela half mir dabei, das passende Material dafür zu finden.

Jenseits der professionellen Unterstützung möchte ich die emotionale Unterstützung in meinem persönlichen Umfeld nicht übersehen. Die Hilfe und Ermutigung, die ich von so vielen wunderbaren Menschen erhalten habe, haben diesen Meilenstein für mich möglich gemacht. Ich bin meiner Familie, Angelika, Michael, Matthias und Markus, zutiefst dankbar. Zusätzlich möchte ich Siegfried, Anna und Ester für ihre Unterstützung erwähnen und mich bei ihnen bedanken.

Content

List of abbreviations

AYCF	Ablation Yield Correction Factor
CCD	Charge-coupled devices
CRC	Collision Reaction Cell
DA	Decoloring Agent
HCA	Hierarchical Cluster Analysis
ICCD	Intensified CCD
ICP-MS	Inductively Coupled Plasma-Mass Spectrometry
ICP-OES	Inductively Coupled Plasma-Optical Emission Spectrometry
IR	Infrared
KED	Kinetic Energy Discrimination
LA-ICP-MS	Laser Ablation-Inductively Coupled Plasma-Mass Spectrometry
LIBS	Laser-Induced Breakdown Spectroscopy
LOD	Limit of Detection
MD	Mean Deviation
OCSVM	OneClass Support Vector Machine
PCA	Principal Component Analysis
PMT	Photomultiplier Tubes
RBF	Radial Basis Function
RM	Recycling Marker
RSD	Relative Standard Deviation
SD	Standard Deviation
SEM-EDS	Scanning Electron Microscopy-Energy Dispersive Spectrometer
SVM	Support Vector Machine
XRF	X-Ray Fluorescence
YAG	Yttrium Aluminum Garnet

1 Introduction

By provenancing the origin of the raw materials of an artifact found at a specific location, structures of the antique industry can be unveiled. In combination with archaeological information on the analyzed artifacts, trading routes can be established, which is crucial in understanding the economic system of a society. Each raw material has a distinct geological signature, which can be linked to the origin of the material and is called the chemical fingerprint. [1] This chemical fingerprint can be assessed using different elemental analysis methods.

1.1 Comparison of Analytical Techniques

When examining historical glass artifacts, Laser Ablation-Inductively Coupled Plasma-Mass Spectrometry (LA-ICP-MS) stands as the established method, having supplanted the previous practice of liquid measurement, that requires glass sample digestion. Other solid state analysis methods are used regularly in archaeological sciences, e.g. X-Ray Fluorescence (XRF) or Scanning Electron Microscopy (SEM) in combination with an X-Ray Energy Dispersive Spectrometer (EDS). LA-ICP-MS offers a distinct advantage over SEM-EDS and XRF by providing access to trace elements with impressively low detection limits. Moreover, the topmost layer of the material under analysis can be swiftly eliminated just prior to the measurement, thereby granting access to the underlying regions for the examination. Furthermore, it stands out as the only method capable of providing isotopic information about samples, while opening up the entire periodic table for quantification, while X-Ray excitation-based methods are usually limited to elements heavier than Na. [2], [3] Figure 1.1 visualizes the differences of the detection limits of some of the commonly used analytical techniques. [4]

The motivation behind this study is to explore the benefits of incorporating Laser-Induced Breakdown Spectroscopy (LIBS) into the analysis process, by using a Tandem-LIBS-LA-ICP-MS configuration. While in general this method provides full elemental coverage, including elements that can be challenging to measure or are entirely inaccessible with ICP-MS, LIBS especially stands out for the analysis of glass, because of its high sensitivity towards alkali and earth alkali elements, which are major and minor components in glass materials. Also, it can be used for non-targeted analysis, making it well-suited for analyzing material with unknown compositions. Furthermore, LIBS can be utilized in portable systems, offering practical advantages for fieldwork. Using LIBS for quantification has in general been proven difficult in the past mainly because of matrix effects. In this study, the sum normalization method is

employed for the quantification of glass using LIBS, aimed at evaluating its potential for achieving more precise quantification outcomes.

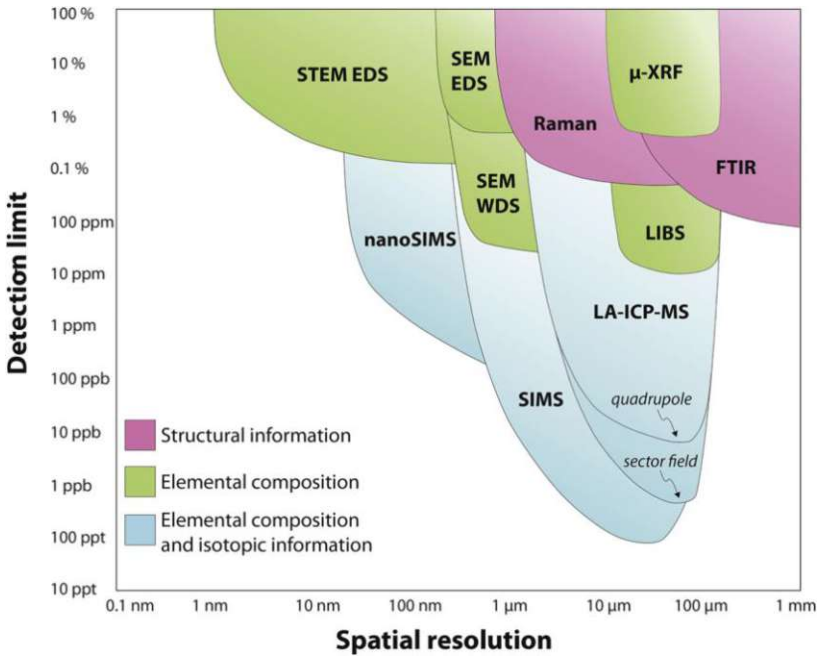

Figure 1.1: Visualization of the detection limits of the mentioned analytical techniques; from [4]

After completion of the elemental analysis, the obtained data must be processed and statistically evaluated to be able to classify the samples and give insight into its provenance. In the literature different methods have been tried out, assessing different elements and element groups. Different components are plotted against each other and compared to previously analyzed samples. This is all done visually by grouping samples in 2D biplots. When a lot of samples are assessed together and no prior knowledge about the samples is present, the problem arises, that no glass groups established in the literature can be excluded, and the formation of data clouds in 2D biplots becomes increasingly difficult. This is where the application of Machine Learning becomes relevant. Models like k-Nearest Neighbor (k-NN) and Support Vector Machines (SVM) can be trained using reference data to classify incoming data. This approach will be explored in the forthcoming study to determine the provenance of late-antique glass samples.

1.2 Samples from Hemmaberg, Austria

The 46 samples to be analyzed were provided by the Austrian Archaeological Institute (ÖAI). They were excavated at the excavation site of Hemmaberg in Carinthia, Austria. Hemmaberg is situated on a low hill, close to the Slovenian border in the foothills of the Karawanks. A series of systematic excavations, ongoing since 1978, have yielded evidence of habitation at this location dating back to the Neolithic period. [5] Investigations conducted on the eastern portion of the plateau uncovered structures from the late antique era, including five churches, at least three substantial residential buildings, and three smaller structures that could potentially be interpreted as cisterns. [6]

Overall, the samples showed a range of blue, green and brown shades, with the majority being colorless or only lightly colored. They were highly fragmented and most of the artifacts' original use could not be recognized. Among these, six samples are potentially unformed primary glasses. The sampling of the artifacts, a subset of which is depicted in Figure 1.2, was carried out together with the archaeological scientist Pamela Fragnoli from ÖAI. Detailed information regarding the artifacts gathered during the examination, is documented in Table 9.1 in the *Appendix*, along with accompanying photographs of all the artifacts.

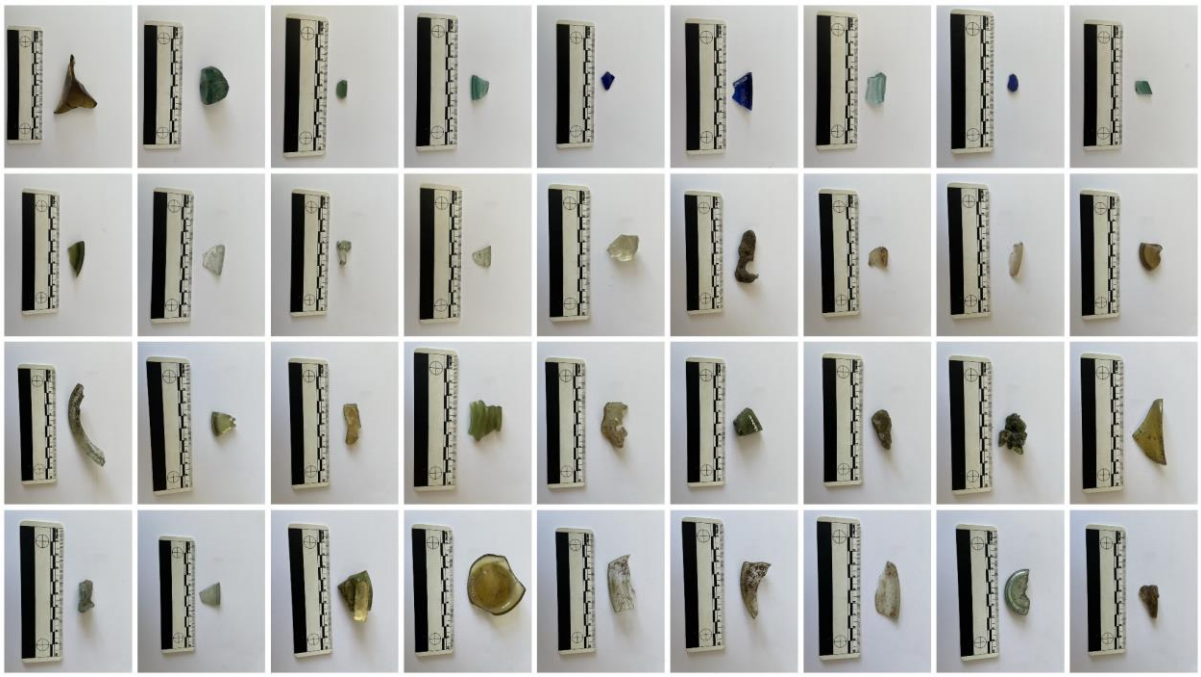

Figure 1.2: Subset of the sampled artifacts, illustrating the range of color and form

2 Theoretical Background

2.1 The Investigated Material from a Modern Perspective

The term glass used in a colloquial context mainly refers to so-called soda lime silicate glass, made of sand (SiO_2), limestone ($CaCO_3$), and soda ash (Na_2CO_3), which makes up the majority of the commercially produced glass in modern times. [7] However, in the scientific world, the definition of glass is much broader, as it includes various materials with different compositions. The "International Commission on Glass" defines glass in the following way:

> *The term "glass" refers to a state of matter, usually produced when a viscous molten material is cooled rapidly to below its glass transition temperature, with insufficient time for a regular crystal lattice to form.* [8]

Besides the before-mentioned soda lime silicate glass, there are glasses with different major components. An exemplary outtake is: [7]

- Borosilicate glass with small amounts of alkali added to silica and boron oxide, which has a low thermal expansion coefficient and a high resistance to chemical attacks.
- Within the group of Aluminosilicate glasses, one differentiates between alkali-free alkaline earth aluminosilicate glasses, which show high electrical resistance, and alkali-containing aluminosilicate glasses, which can yield ultrahigh strength glass products.
- Lead silicate glass consists mainly of PbO and SiO_2, with small amounts of soda or potash. It is characterized by its high brilliance, high electrical resistivity, and large working range.
- When melting chalcogen elements with one or more of groups 14 and 15 elements the chalcogenide glasses are obtained. They are utilized for their semi-conducting (switching) behavior, photoconductivity, and IR-transmitting properties.

2.2 The Investigated Material from an Archaeometric Perspective

There has been evidence for the production and use of small glass objects, such as beads and pendants, back until the late third millennium BC, whereas the production of larger glass vessels seems to have begun in the late sixteenth century to mid-fifteenth BC in Northern Syria/Mesopotamia and Egypt. During this time, the mostly strongly colored glass was still considered a luxurious good. With the invention of glass blowing in the first century BC, which occurred in Syria-Palestine, the production of glass was much more commercialized and the products were exchanged all over the Roman empire. By the mid- to late first century AD blown, transparent glass in weaker "natural" colors and decolorized glass, was widespread for the use as dishes, for storage and for windows. [9]

The raw glass was produced in so-called primary workshops in large furnaces, where several tons of glass were produced in one firing. Such furnaces have been excavated in the Levant in Bet Eli'ezer, Israel (7th-8th century AD), Beth She'arim, Israel (early 9th century AD), Apollonia, Israel (6th-7th century AD), and Tyre, Lebanon (10th-11th century AD). [9] In Egypt, furnaces have been found on the shores of Lake Maryut (1st to 8th century AD) and at Wadi Natrun (1st-2nd century AD). From these primary production sites, the raw glass was shipped off to the so-called secondary workshops, which were located all over the Roman Empire. Here the glass was remelted and formed into the desired shape. [1]

Roman natron glass can basically be seen as a mixture of three main ingredients: silica sand, a lime-bearing mineral, and a soda-rich flux. Also, certain elements were introduced into the material for (de-)colorization (see *Recycling*). An overview of the link between elements and the raw materials utilized is provided in Figure 2.1.

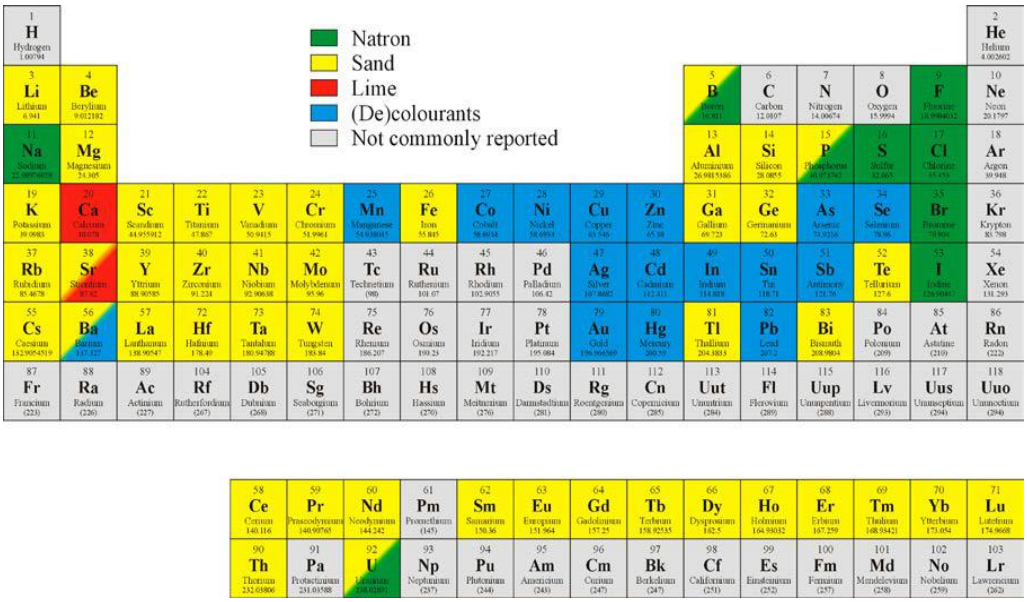

Figure 2.1: Periodic table showing the most likely sources of the elements occurring in natron glasses; from [1]

The majority of the glasses produced in the Roman world were soda-lime-silica glasses. They could be differentiated by the main flux ingredient: mineral soda (natron) or plant ash. The natron glasses can be characterized by low magnesium and low potassium levels (MgO, K_2O < 1.5 wt%), and the plant ash glasses by their high magnesium and high potassium levels (MgO, K_2O > 1.5 wt%). [1]

2.2.1 Recycling

The Romans already took advantage of the fact that glass can be remelted and reused multiple times. Archaeological evidence for recycling is provided by found large collections of cullet, for example in a Roman villa in Italy or also in the body of the shipwreck “Iulia Felix” found at the coast of Grado, Italy. Also, there is documentary evidence by Roman poets such as Strabo and Martial, who describe men roaming the streets collecting broken glass in exchange for sulfur matches. [10]

Now on to the analytical evidence: To find out if the samples are possibly recycled, various Recycling Markers (RM) have been established in the literature. On the one hand, one can look at the so-called Decoloring Agents (DA). Historically, in ancient times, either Manganese- or Antimony oxide served as such agents. These substances have been added to the glass batch in the primary glassmaking step, when mixing sand and alkali, oxidizing the Fe^{2+} to the practically colorless Fe^{3+}. If both of these decolorizers are detected in a glass artifact simultaneously, above a certain threshold, the glass is believed to be recycled. [11], [12]

On the other hand, there are certain trace elements, which have been added to the glass as chromophores (Co, Cu, Fe) or are accompanying one of the chromophores (Zn, Sn, Pb). If one of these elements is detected between 100 µg/g and 1000 µg/g in naturally colorless or colorless glass, this is also a sign of recycling. [13]

2.3 Analysis Methods

The two methods, which were combined in a Tandem-measurement, are LIBS and LA-ICP-MS. As the laser plays a key role in this set up the first sub-chapter will discuss the basic properties of lasers and their use in analytical chemistry, before explaining the two combined methods separately.

2.3.1 The Laser and its Use as an Ablation Technique

The term “Laser” is an acronym for Light Amplification by Stimulated Emission of Radiation. To understand how lasers work, it's important to grasp the principles of excitation. When a photon is absorbed by an atom or molecule, two processes can lead to the emission of photons: spontaneous emission (random direction) and stimulated emission (two identical photons with the same wavelength and direction). [14] According to the Boltzmann distribution when atoms are in thermal equilibrium the majority of them exist in the ground state. Achieving a population inversion, where more constituents occupy excited states than the ground state, is essential for light amplification through stimulated emission, typically achieved through pumping. Gas lasers, such as Excimer lasers, use impact energy, while solid state lasers, like Nd:YAG lasers, use external electromagnetic radiation to transfer the necessary pump energy to the gain medium. [15] Figure 2.2 highlights the difference between radiation passing through a noninverted population and an inverted population, enabling the light amplification used in a laser.

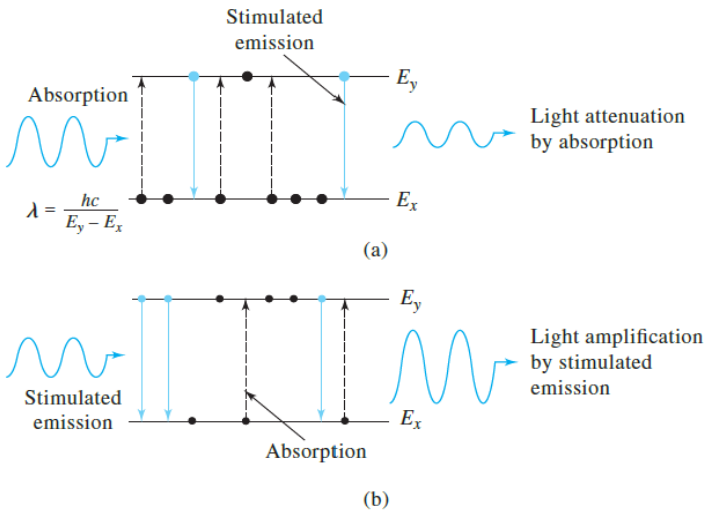

Figure 2.2: Radiation passing through a (a) non-inverted population and (b) an inverted population; from [14]

Laser sources have become an important tool in analytical chemistry because of their high intensities, the high monochromaticity and the coherence of the emitted light, achieved by making use of the phenomena previously described. [14]

The most commonly used are Nd:YAG lasers and Excimer lasers. The Nd:YAG laser is a solid state laser, where the lasing medium consists of a neodymium ion in a host crystal of yttrium aluminum garnet. The fundamental wavelength of Nd:YAG lasers resides in the near-IR range, precisely at 1064 nm. Wavelengths of 532, 355, 266, and 213 nm could be achieved with the help of optical frequency doubling tripling, quadrupling, and quintupling. Excimer lasers incorporate a gas mixture comprising He, F, and one of the rare gases, such as Kr, Ar, or Xe. These rare gases are electrically excited through a current and subsequently react with fluorine, resulting in the formation of excited species known as excimers, which remain stable exclusively in their excited state. The Excimer lasers' wavelength is determined by the operating gas (XeCl 308 nm, KrF 248 nm, ArF 193 nm, F_2 157 nm). [14], [16]

While the advantages of direct-solid sampling have become more investigated, the use of Laser ablation in analytical chemistry has grown fundamentally over the past years. A laser beam focused on the sample surface is used to sample a minimal volume of the specimen under investigation. The wavelength of the laser is a critical factor influencing the ablation process. Shorter wavelengths have been observed to result in more efficient ablation due to the higher energy density, which aids in breaking chemical bonds, and less influence by plasma shielding. Plasma shielding, a phenomenon occurring during ablation, involves the absorption or reflection of a portion of the laser energy by the laser-induced surface plasma. Longer wavelengths exhibit greater absorption, ergo leading to less efficient. Furthermore, apart from the wavelength of the laser source the pulse duration also plays a major role in the ablation behavior. Femtosecond laser pulses improve the ablation efficiency and minimize thermal effects and plasma shielding compared to nanosecond laser pulses. [17], [16]

2.3.2 LIBS

When the laser is shot onto the surface, material is ablated, but at the same time, a partially ionized short-lived plasma is formed, which contains excited ions and atoms. As the plasma cools down, the deexcitation of these atoms and ions emit an emission spectrum during the first hundreds of nanoseconds, making the time of observation a significant factor to consider. Typical instrumentation can be seen in Figure 2.3. The element-specific radiation, emitted as the excited states of the atoms or ions in the plasma decay, is collected by fiber optics and transferred to a spectrometer. To detect the emitted light photomultiplier tubes (PMT) are used commonly, as they are compact, highly sensitive, and relatively inexpensive. When a

two-dimensional detection of the light incident is needed, Charge-coupled devices (CCD) are used, among others. While the use of a PMT is limited to the detection of selected lines, a CCD enables a full spectra acquisition. The collected LIBS spectrum contains element-specific lines, which can be used for qualitative and quantitative analysis. [18]

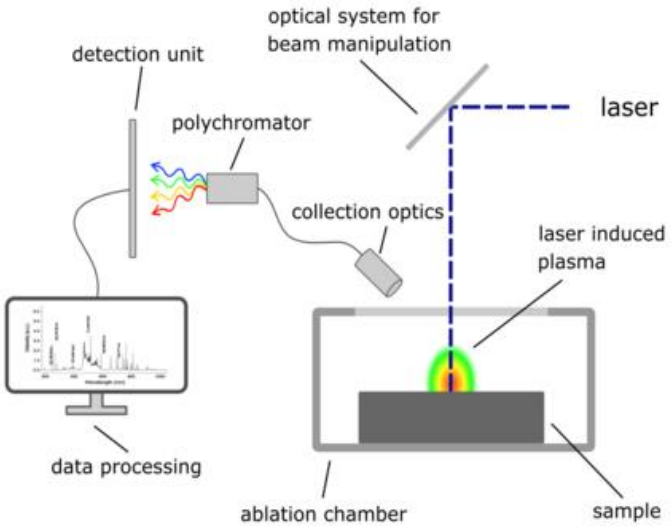

Figure 2.3: Schematic instrumentation for LIBS

In quantitative analysis, LIBS encounters difficulties due to spectral overlapping, self-absorption, and so-called matrix effects. The matrix represents all components other than the analyte, and its variations can influence the ablation, atomisation, ionization and excitation of the material and the formation of the plasma. These factors mentioned beforehand can lead to non-linear relationships between the quantities being measured and the corresponding spectral signals. Therefore, in order to ensure similar ablation conditions and minimize matrix effects, it is essential to use standards with a base composition that closely resembles the sample of interest, so-called matrix-matched standards. [19]

LIBS offers several advantages as an analytical technique. Firstly, it allows for the simultaneous analysis of multiple elements, making it efficient and time-saving for obtaining comprehensive elemental information in a single measurement, while accessing all elements of the periodic table. Secondly, LIBS is a fast method, providing real-time results with minimal sample preparation, which is advantageous for quick analysis in various applications. Regarding the analysis of glass samples, LIBS demonstrates exceptional sensitivity towards alkali and earth alkali elements, making it highly suitable for studying the composition of

glasses. However, there are some limitations to consider. LIBS may exhibit insensitivity towards trace elements, making their detection challenging. Additionally, the quantification of results can be difficult, as mentioned beforehand. [19]

2.3.3 LA-ICP-MS

In LA-ICP-MS the material ablated by the laser is transported by a carrier gas flow (commonly He) into the ICP unit. In the plasma, the solid material is vaporized, atomized, and ionized. The ion beam is transferred from atmospheric pressure to high vacuum through an interface consisting of a sampler and skimmer cone. Ion optics shape the beam before entering the mass analyzer, where the ions are separated by their mass-to-charge ratios. The three most common mass analyzers are the quadrupole, the sector field, and the time of flight mass spectrometer. The most frequently applied system, the quadrupole, works in the following way. Four cylindrical rods, that serve as electrodes, are connected pair-wise to radio frequency and direct current voltage. Sequentially and fast different voltages can be applied and ions of only one mass-to-charge ratio will pass through, while all others strike the rods and are converted to neutral molecules. Despite the limitation of sequential measurement and unit mass resolution the quadrupole stands out in comparison to the other mass analyzers by being compact, less expensive and more robust. [20]

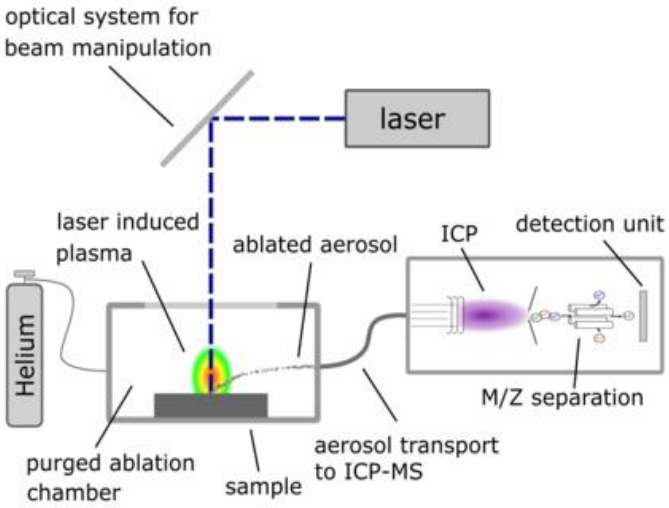

Figure 2.4: Schematic instrumentation for LA-ICP-MS

Ions with a similar mass-to-charge ratio or the formation of polyatomic ions with a similar mass-to-charge ratio to the analyte can lead to interferences during the measurement. In order to eliminate spectral interferences in quadrupole ICP-MS, Collision Reaction Cells (CRCs) have been introduced. In Collision mode these cells employ a non-reactive gas and a technique called kinetic energy discrimination (KED) to minimize polyatomic interferences. KED makes use of the fact, that all formed polyatomic ions must be larger in size than the atomic analyte, resulting in more frequent collisions with the gas and ergo the reduction of their kinetic energy. By applying an energy barrier at the exit of the cell, polyatomic interference are removed from the ion beam. The so-called Reaction mode utilizes a specific reaction gas to eliminate known, reactive interferences from each analyte isotope. [21]

Despite becoming an established standard procedure, with detection limits in the µg/g or even ng/g range for some elements, which also enables isotopic analysis, LA-ICP-MS still has some significant limitations. Due to the transient nature of the signals generated with laser ablation, which hinders the detection of full spectra in the sequential operation mode of a quadrupole mass spectrometer. This limitation necessitates a prior definition of the analytes to be analyzed, requiring prior knowledge about the sample. The monitored mass-to-charge ratios are limited, so multi-elemental analysis is only possible to some extent. Moreover LA-ICP-MS exhibits low sensitivity to non-metals, making their detection challenging with this technique. Additionally, during the transportation of material from the ablation cell to the ICP unit, there is a risk of material loss, potentially affecting the accuracy and precision of the analysis. [19] Also for LA-ICP-MS the beforementioned matrix effects pose challenges for accurate quantifications.

2.3.4 Tandem-LIBS-LA-ICP-MS and its Advantages

Having discussed the two methods individually, we will now delve into the coupling of LIBS and LA-ICP-MS, known as Tandem-LIBS-LA-ICP-MS. This powerful pairing allows to combine the simultaneous multi-elemental capacity of LIBS and the ability of LA-ICP-MS to detect trace elements. In that way the information gained from one single measurement increases immensely. However, it is important to consider that when combining these techniques, compromises must be made regarding the laser parameters. This methodology works in a way that when the laser is shot onto the sample surface, the emitted light is collected to obtain the LIBS spectrum, and within milliseconds, the aerosol containing the ablated material is transported to the ICP unit.

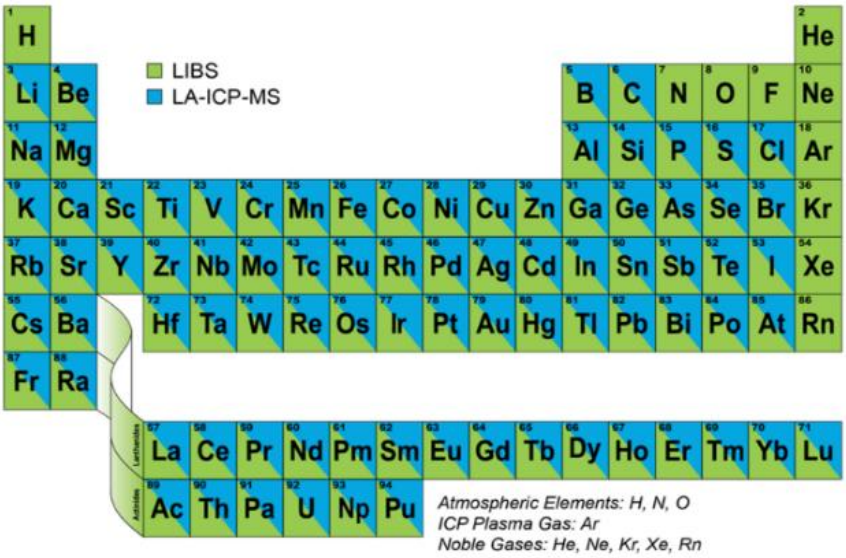

Figure 2.5: Overview of the capacity of multi-elemental analysis with Tandem-LIBS-LA-ICP-MS; from https://www.icpmslasers.com/products/eslumen/ [Accessed: 12.09.2023, 16:00]

Regarding advantages, it can be stated that direct solid sampling is less laborious and minimally invasive compared to the required digestion of the material for liquid measurement. On the other hand, representative reference materials are needed to enable quantification with direct solid sampling. Nevertheless, the implementation of Tandem measurements enables a multi-elemental analysis covering the entire periodic table (see Figure 2.5). Moreover, regarding quantification, this technique provides the capability to analyze a concentration range that extends from percentages to nanograms per gram.

2.4 Machine Learning Algorithms for Classification and Clustering

In Machine Learning one can differentiate between supervised and unsupervised machine learning algorithms. If the model is trained with pairs of input data and the desired output beforehand it is called supervised. The two major types of supervised machine learning problems are classification and regression. On the other hand, for unsupervised algorithms, only the input data is known. An example of an unsupervised machine learning problem is clustering. [22]

Before explaining the used methods in detail, general remarks have to made about classifiers and their usage in chemometrics. When developing a classifier with analytical data, it is important to follow a certain procedure to ensure the quality of the model. After acquiring the data, it is typically split into a training set (about 80 %) and a test set (about 20 %). The data then undergoes preprocessing, which includes background correction, normalization and, if necessary, spectral noise removal. Furthermore especially for techniques like LIBS, which generate spectra with thousands of data points, it is important to carefully select variables. For qualitative analysis this means extracting specific element lines' intensities or integrated spectral regions as so-called spectral descriptors. This step reduces dimensionality and avoids the "curse of dimensionality" and overfitting by extracting relevant information instead of utilizing the entire spectrum. Once the data is prepared, the model is constructed and tested with the test set. If necessary, the training process may be repeated until achieving a satisfactory level of model quality. [23]

By testing the model with unseen data, one can make sure that the model generalizes well. If the model is excessively complex and fits the training data too closely, it can lead to overfitting, causing poor performance on test data. On the other hand, if the model generalizes too much, it may underfit. Thus, finding the right balance between overfitting and underfitting is crucial for optimal model performance. [22]

2.4.1 OneClass-Support Vector Machines (OCSVM) for Novelty Detection

Support Vector Machines (SVM) are supervised learning classification models. A hyperplane is used as a decision boundary between different classes. A way to allow this linear classifier the classification of data, even when the data is not linearly separable, is to apply the so-called kernel trick. This technique involves mapping the data points into a higher-dimensional space by transforming them mathematically. The most commonly used are the polynomial kernel and the radial basis function (RBF). [22] For the performance of the model, it is crucial to find the optimal margin of the hyperplane, which is the minimal distance between the hyperplane and the closest data points. [24]

The One Class-SVM (OCSVM) is an extension of the method described beforehand. This technique is employed for the so-called Novelty Detection in data, whereby the objective is to identify data points that show significant deviations from the rest of the data. Here the input data is regarded as a single class, while the unknown data points will be classified either as part of this class or as an outlier. [25]

2.4.2 k-nearest Neighbor Algorithm (k-NN)

The k-NN algorithm is a supervised learning classification model. It classifies an unknown data point by assigning it to the k closest neighbors based on a specific distance measure. The Euclidean distance is commonly used to determine the vicinity of the neighbors. Finding the optimal k-value is crucial. The hyperparameter can be optimized by cross-validation. The decision is typically made through Majority Voting, where the class label assigned to the unknown data point is determined by the majority class among its k nearest neighbors. [22]

2.4.3 Hierarchical Cluster Analysis (HCA)

Hierarchical clustering, an unsupervised learning method, initially treats each data point as an individual cluster. Then the clusters are progressively merged until a predefined stopping criterion is met, which typically is the number of clusters. Clusters are merged depending on the selected linkage method. For instance, complete linkage merges the two clusters that show the smallest maximum distance between any pair of their data points. On the other hand, average linkage merges the two clusters that possess the smallest average distance across all points within the clusters. Dendrograms are used for the visualization of HCA. [22]

2.4.4 Principal Component Analysis (PCA)

PCA is an unsupervised learning method used as an exploratory data analysis tool. Its main purposes are data visualization and data compression. In PCA, information from multiple variables is combined into a smaller set of orthogonal variables known as principal components. These principal components are linear combinations of the original indicators, chosen in a way that captures the most variance in the data. By reducing the dimensionality of the data, PCA aids in understanding patterns and relationships within complex datasets. [26]

3 Experimental

3.1 Reagents, consumables and instruments

Before diving into the experimental part of this thesis, the instruments, reagents and consumables used regularly during the daily laboratory work should now be listed separately to ensure a better readability. First the used chemicals and their supplier is listed in Table 3.1. Furthermore, a list of used consumables can be found in Table 3.2.

Table 3.1: List of used chemicals

Name	*Additional information*	*Supplier*
Argon	99,999% UN1006	Messer, Gumpoldskirchen, Austria
Epoxy resin, two components	EpoFix Kit UN33082, UN2259	Struers, Willich, Germany
Ethanol	≥99.9%, p.a. EMSURE®	Merck, Darmstadt, Germany
Helium	≥99.999 Vol% UN1046	Messer, Gumpoldskirchen, Austria
Hydrochloric acid	37 %, p.a. EMSURE®	Merck, Darmstadt, Germany
Hydrofluoric acid	40 %, Suprapur®	Merck, Darmstadt, Germany
Nitric acid	65 %, p.a. EMSURE®	Merck, Darmstadt, Germany
Nitrogen	99,999 Vol% UN1066	Messer, Gumpoldskirchen, Austria
Silicon Carbide Paper	#320, #1000, #4000	Struers, Willich, Germany
Thermoplastic adhesive	-	Struers, Willich, Germany

Table 3.2: List of consumables

Name	*Additional information*	*Supplier*
Antistatic weighing boat	-	VWR, Darmstadt, Germany
Centrifuge tube w. screw cap	50 mL	VWR, Darmstadt, Germany
Centrifuge tube	15 mL, 12500 g	VWR, Darmstadt, Germany
Centrifuge tube	15 mL, 20000 g	VWR, Darmstadt, Germany
PFA digestions vial	-	VWR, Darmstadt, Germany
Pipette tips, various sizes	epT.I.P.S.®	Eppendorf AG, Hamburg, Germany
Polypropylene spatula	-	VWR, Darmstadt, Germany

Additionally, a list of instruments used regularly for the completion of this work can be found in Table 3.3. The water used for laboratory work, which has been prepared with the EASYPURE II water system will from now on be referenced as Milli-Q water.

Table 3.3: List of regularly used instruments

Name	*Supplier*
Analytical balance ENTRIS® II BCE224I-1S	Sartorius, Göttingen, Germany
EasyDigest® heating block	Analab, Paris, France
EASYPURE II water system for ultrapure water with a resistance of 18.2 MΩcm	Thermo Scientific, Bremen, Germany
Multiwave 5000 Microwave System with PTFE-TFM microwave vessels and SVT50 rotor	Anton Paar, Graz, Austria

The used Microwave system together with the SVT50 rotor containing the PTFE-TFM vessels by Anton Paar, Austria is depicted below in Figure 3.1.

Figure 3.1: Multiwave 5000 microwave system (Anton Paar); from https://www.anton-paar.com/at-de/produkte/details/multiwave-5000/ [Accessed: 02.11.2023, 16:00]

Furthermore, two solid reference glasses were used, namely NIST® SRM® 610 and NIST® SRM® 612, by the National Institute of Standards and Technology, Gaithersburg, USA. For the liquid analysis various standard solutions were used, all of which are listed in the *Appendix*.

3.2 Solid Measurements: Tandem-LIBS-LA-ICP-MS

3.2.1 Sample Preparation

To keep most of the sample possible unharmed by the analysis it had to be cut. For smaller fragments, this could be achieved by small, controlled hammer strokes. For the bigger samples, the glass was glued onto a metal plate with thermoplastic adhesive and cut with a glass-cutting machine (see Figure 3.2). To obtain the separated piece the adhesive was removed with Limonene. Afterwards, the samples were embedded in epoxy resin, left to dry for about 12 hours, sanded and polished (see Figure 3.3).

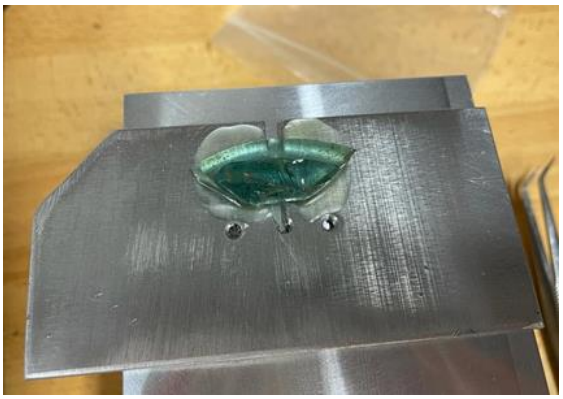

Figure 3.2: Sample fixed on metal plate before cutting

Figure 3.3: Selection of embedded samples

While a few samples were sanded and polished manually most of them were sanded with a sanding machine (Struers Tegra System: TegraPol-31, TegraForce-5, TegraDoser-5) with Silicon carbide sanding paper. All samples were investigated under the microscope before measurement. These microscopic images can be found in the *Appendix*.

3.2.2 Measurement with Tandem-LIBS-LA-ICP-MS

For the Tandem-measurement the ImageGEO193 Laser Ablation system (Elemental Scientific, USA) with an ArF-Excimer Laser operating at a wavelength of 193 nm in combination with the ESLumen – Multichannel detector (Elemental Scientific, USA) and the iCAP Qc ICP-MS (Thermo Scientific, Germany) was used. The ablation chamber, equipped with the analytical cup wit LIBS abilities, was connected to the ICP unit with a Tygon® tubing with an inner diameter of 3.2 mm. Before the measurement the ICP-MS system was tuned using NIST® SRM® 612 for a maximum ^{115}In signal. The reference material NIST® SRM® 610 was used to optimize the laser settings. The detailed measurement conditions can be found in Table 3.4.

Table 3.4: Measurement conditions for the solid measurement

LIBS and laser settings	
Chamber gas flow	He, 0.8 L/min
Spot size	100 x 100 µm^2
Pattern design	30 spots/sample
Laser energy	100 % (1.1 mJ)
Laser repetition rate	20 Hz
Number of shots/spot	200
Warmup time	0 s
Washout delay	4 s
Software	ActiveView2 (Elemental Scientific, USA)
ICP-MS	
Plasma power	1500 W
Dwell time/isotope	0.01 s
Ar make-up flow	0.8 mL/min
Cool gas flow	14 mL/min
Auxiliary gas flow	0.8 mL/min
Measured isotopes	^{7}Li, ^{27}Al, ^{29}Si, ^{31}P, ^{34}S, ^{39}K, ^{43}Ca, ^{45}Sc, ^{55}Mn, ^{56}Fe, ^{59}Co, ^{65}Cu, ^{66}Zn, ^{86}Sr, ^{89}Y, ^{92}Zr, ^{109}Ag, ^{112}Cd, ^{118}Sn, ^{121}Sb, ^{138}Ba, ^{139}La, ^{140}Ce, ^{141}Pr, ^{144}Nd, ^{158}Gd, ^{174}Yb, ^{197}Au, ^{208}Pb, ^{209}Bi
Software	Qtegra (Thermo Scientific, Germany)

All measurements were carried out in batches of 7 samples, and two reference materials: NIST® SRM® 610 and NIST® SRM® 612. This was easily achieved by using the specimen holder

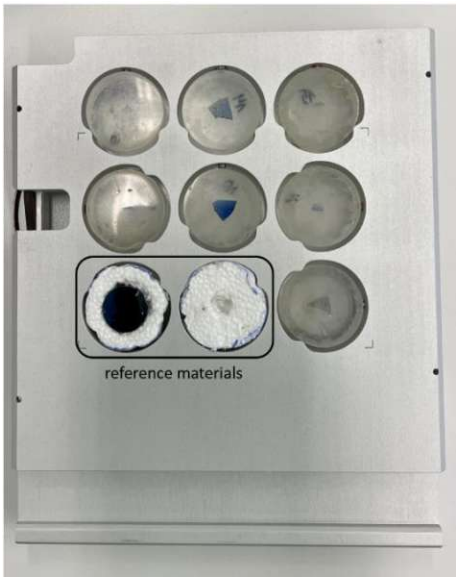

Figure 3.4: Specimen holder with two reference materials and seven samples

seen in Figure 3.4, where the embedded samples could be placed conveniently at the same height.

In addition to the bulk measurements, three samples were selected for a comprehensive surface imaging analysis. The specimens were covered with a grid of 50 µm x 50 µm laser shots with zero overlay, at a frequency of 100 Hz, using 100 % laser energy and 0 s offset.

3.2.2.1 Determination of Depth of Analysis with a Profilometer

To get insight into the depth of the analysis and the form of the laser crater the two reference materials and two samples were examined with a DektakXT® stylus profilometer (Bruker, USA) after completing the measurements. The results can be seen in Figure 3.5 below.

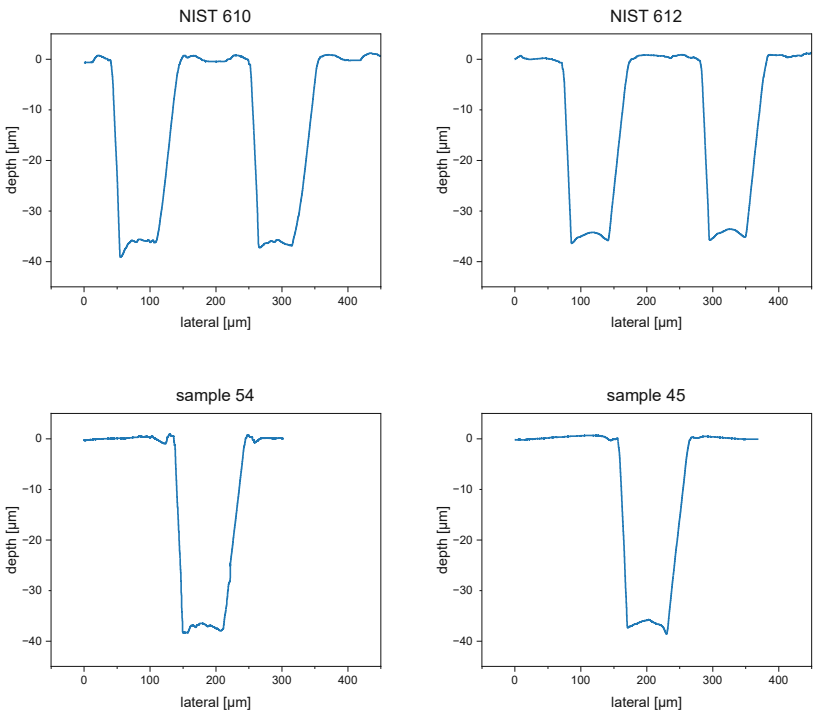

Figure 3.5: Results of the analysis of the laser craters with a profilometer

As one can see the shot laser craters show the desired rectangular shape and a regular depth of 35-40 µm. This outcome is favorable, because the close resemblance of the ablation behavior of the materials enables effective utilization of the reference materials for an accurate sample quantification.

3.2.3 Quantification and Pre-Processing

The acquired data was imported into iolite v4. The ICP-MS data was synchronized with the laser logfiles. Selections for each sample and reference material were created. The data was background corrected and normalized by the reference materials measured before and after each sample batch. The Trace Element Data Reduction Scheme, featured in iolite, was employed for semi-quantitative analysis.

The LIBS-data was imported using the LIBS importer tool. Two different quantification approaches were attempted. Firstly, the semi-quantitative method was employed, similarly to the procedure used for the ICP-MS data. Additionally, the sum normalization method, integrated in the software and based on the model of Liu et al. [27], was utilized in various iterations. This method is based on the normalization of all contained oxides to 100 wt%, applying the so-called ablation yield correction factor (AYCF). This allows the correction of the matrix-dependent absolute amount of materials ablated during each run. This approach eliminates the necessity for an internal standard. [27]

In total, five different iterations were conducted, each time utilizing different element lines. Further details regarding the specific element lines employed can be found in Table 3.5.

Table 3.5: Variants used for method of sum normalization

quantified element	*variant 1*	*variant 2*	*variant 3*	*variant 4*	*variant 5*	*variant 6*
Na	Na518	Na588	Na518	Na518	Na518	Na518
Mg	Mg285	Mg285	Mg285	Mg285	Mg280	Mg280
Al	Al396	Al308	Al396	Al396	Al394	Al394
Si	Si288	Si288	Si288	Si288	Si288	Si251
K	K769	K769	K769	K769	K769	K769
Ti	Ti308	Ti308	Ti308	Ti308	Ti308	Ti308
Ba	Ba493	Ba493	Ba493	Ba493	Ba493	Ba493
Ca	Ca422	Ca422	Ca854	Ca866	Ca866	Ca866
Fe	Fe238	Fe238	Fe273	Fe273	Fe273	Fe273
Mn	Mn259	Mn259	Mn259	Mn259	Mn259	Mn259
Sr	Sr460	Sr460	Sr460	Sr460	Sr407	Sr407

Subsequently, all of the quantification results were subjected to further processing using Python within the Spyder® environment. Data points with a Z-score > 3 were determined as outliers and excluded. Furthermore, a drift correction procedure was conducted for the LIBS data. This involved calculating a factor for each measurement using the total intensity. Equation 1 below illustrates an example of the factor calculation for sample x and

measurement number i. Subsequently, the calculated factor was applied to all element results of measurement i.

$$factor = \frac{total\ int.(measurement\ \#i\ of\ sample\ x)}{total\ int.(measurement\ \#1\ of\ sample\ x)} \qquad \textit{Equation 1}$$

3.3 Digestion and Liquid Measurements

As a reference method to the solid measurement, the glass samples were digested and underwent multi-elemental analysis using conventional liquid ICP-OES and -MS.

3.3.1 Sample Preparation

Beforehand small fractions of selected samples were cleaned by first bathing them in a 1 % HNO_3-solution and then ethanol. After letting them dry they were weighed to about 20-30 mg and crushed mechanically. The now even smaller pieces were weighed accurately (see *Appendix*) and placed into 50 mL PTFE-TFM microwave vessels. 1 mL HNO_3, 1 mL HCl and 4 mL HF were added, and the samples were placed in the rotor SVT50 of an Anton Paar Multiwave 5000 microwave system. The detailed temperature program can be seen in Figure 3.6 and Table 3.6.

Table 3.6: Temperature programs microwave

batch		*Time [min]*	*Temperature [°C]*
1 - 3	ramp	10	180
	hold	35	180
4 - 5	ramp	10	210
	hold	40	210

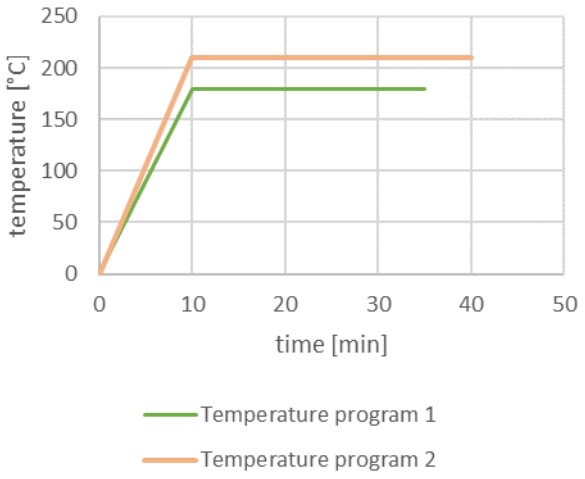

Figure 3.6: Temperature programs microwave

After the first digestion step, some solutions were showing visible precipitate, either in the form of a fine white-grey powder, which was presumed to be fluoride or in the form of bigger

chunks, which was presumed to be incompletely digested glass. To improve the first digestion step temperature program 2 was introduced for batches 4 and 5.

Nevertheless, the digestion was continued with the second step for all the samples equally. The microwave vessels were washed out with Milli-Q water and the washing solution united in PFA digestion vials. The solutions were evaporated to dryness at a temperature of up to 130 °C and the precipitate was taken up with conc. HNO_3 2-3 times. The precipitate of a few samples was insoluble in HNO_3 but was then successfully diluted in conc. HCl. Finally, the residuum was taken up with 2 mL 10% HNO_3 and diluted to 10 mL with Milli-Q water. The following Figure 3.7 gives an overview of the workflow used for the digestion of the glass samples.

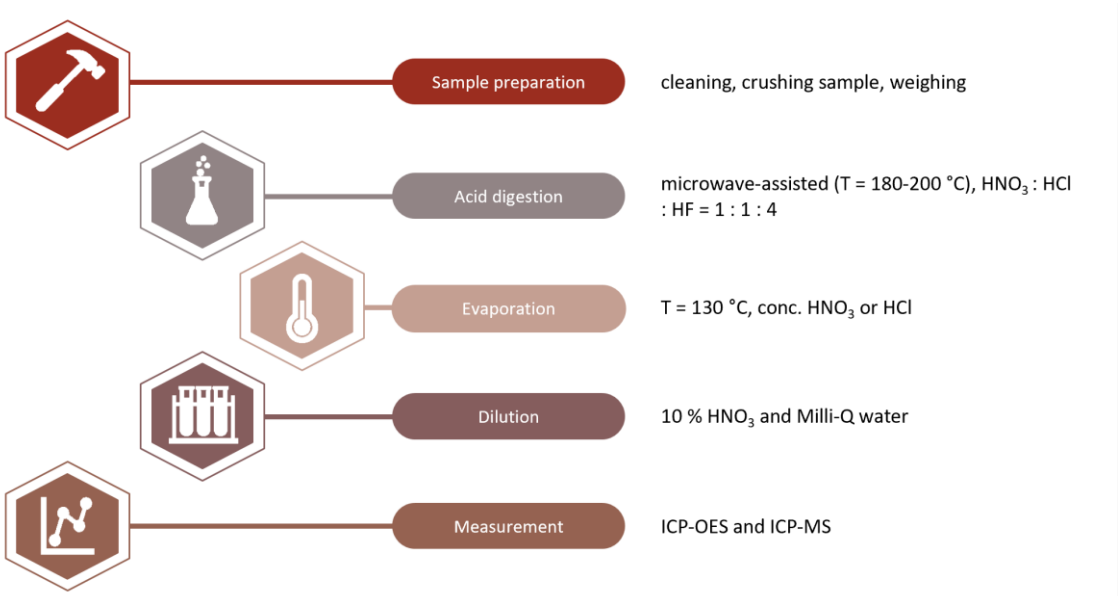

Figure 3.7: Workflow for the digestion of the glass samples

3.3.2 Measurements of the Digested Samples with Liquid ICP-OES and ICP-MS

In the case of liquid measurements, the digested samples underwent analysis using ICP-OES as the initial step. The specific instrument used was the iCAP 6500 RAD (Thermo Scientific, Germany), which was equipped with an ASX-520 autosampler (CETAC Technologies, USA). Emission lines for each element were selected based on prior experiments conducted within this research group. [28] Two different dilutions of the samples were employed: a 1 to 100 dilution for the major and minor components and a 1 to 10 dilution for the trace elements detectable by ICP-OES. For the successful quantification certified standard solutions were used, which are listed in Table 9.2, which can be found in the *Appendix*. For the ICP-OES

measurement a dilution series of the standard solutions was prepared within a concentration range of 0.01 – 2 mg/L was prepared. The detailed measurement conditions can be found in Table 3.7.

Table 3.7: ICP-OES measurement conditions for digested samples

RF Power	1200 W
Nebulizer gas flow	0.75 L/min
Auxiliary gas flow	0.8 L/min
Coolant gas flow	12 L/min
Viewing height	12 mm
Sample flow rate	0.8 mL/min
Integration time	10 s
Number of replicates	3
Internal standard	1 mg/L In
Spectral lines (nm)	Al 396.152, Ba 455.403, Ca 393.366, Co 238.892, Cu 324.754, Eu 381.967, Fe 259.940, K 766.490, La 333.749, Li 670.784, Mg 279.553, Mn 257.610, Na 819.482, Ni 231.604, P 177.495, S 180.731, Sb 206.833, Sc 361.384, Sr 407.771, Ti 334.941, Y 371.030, Yb 289.138, Zn 202.548, Zr 339.198

Elements that were not assessable by OES were successfully quantified with liquid ICP-MS. For that the before mentioned iCAP Qc ICP-MS (Thermo Scientific, Germany) was used, together with an ESI SC-2 DX (Elemental Scientific, USA) autosampler. Standard solutions in a concentration range between 0.01 – 0.1 µg/L were measured, together with the 1 to 100 dilution of the samples. The detailed measurement conditions can be found in and Table 3.8. The combined results of the liquid measurements can be found in the *Appendix*.

Table 3.8: ICP-MS measurement conditions for digested samples

Plasma RF power	1550 W
Dwell time per isotope	0.01 s
Number of Sweeps	50
Sample flow rate	0.4 mL/min
Nebulizer gas flow	1 L/min
Coolant gas flow	14 L/min
Auxiliary gas flow	0.8 L/min
Main runs	4
Measurement mode	KED mode
Internal standard	1 µg/L Eu
Measured isotopes	^{109}Ag, ^{112}Cd, ^{118}Sn, ^{140}Ce, ^{141}Pr, ^{142}Nd, ^{155}Gd, ^{197}Au, ^{206}Pb, ^{209}Bi

3.4 Classification: Statistical Method

For the classification, a multi-step procedure was established. Figure 3.8 displays an organigram to give an overview over this procedure. Over each grey pillar, depicting one step or used algorithm, the analytical method used to obtain the needed data can be seen. The different steps will be explained in more detail in the following chapters.

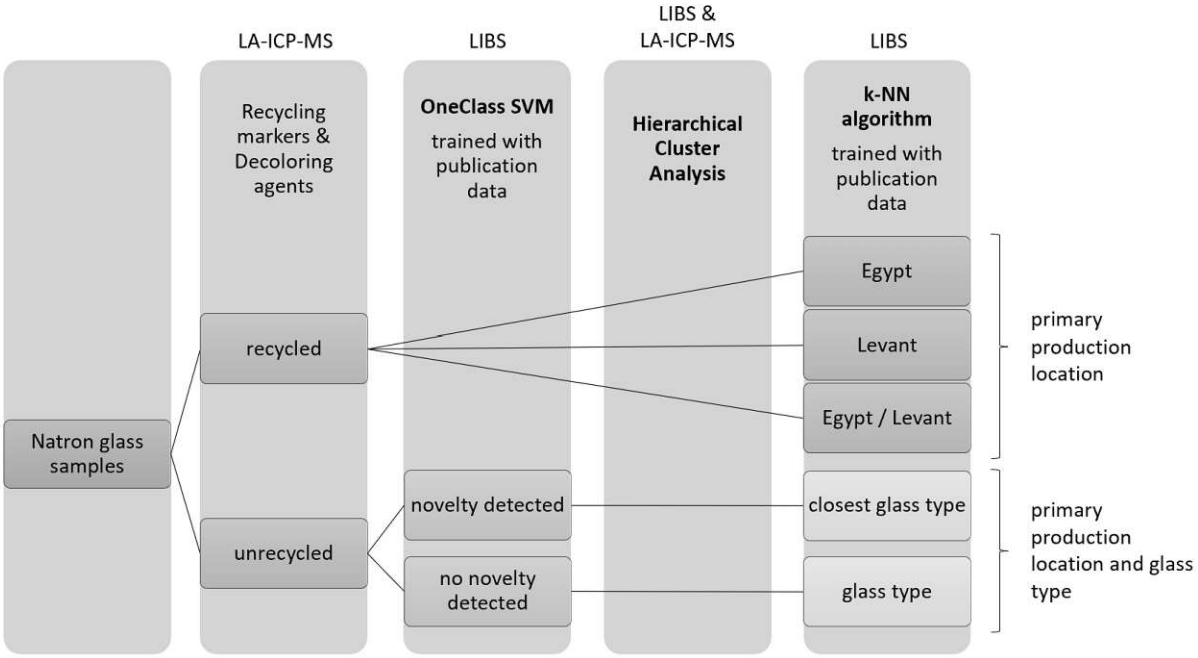

Figure 3.8: Established Statistical Method

3.4.1 Building the Reference Dataset

A reference dataset with about 1500 datapoints, collected from publication data, containing the major and minor components (Al_2O_3, CaO, Fe_2O_3, K_2O, MgO, MnO, Na_2O, SiO_2, TiO_2) of analyzed (late)-antique natron glass samples was built. The glass types which have been included in the database and its origin can be seen in Table 3.9. The statistical analysis was then carried out using Python within the Spyder® environment.

Table 3.9: Reference data for collected database

Included glass types found at different locations	*Number of samples*	*Reference*	*Citation*
Foy 2.1	20	Balvanovic et al. (2020)	[29]
Foy 3.2, Rom/Mn, Rom/Sb	30	Balvanovic et al. (2022)	[30]
Apollonia type, Foy 2.1, Jalame type, Rom/Mn, Rom/Sb	113	Barfod et al. (2022)	[31]

Levantine A, Levantine B, Foy 2	19	Bertini et al. (2020)	[32]
HIMT, Mn a, Sb decolorized	29	Bidegaray et al. (2018)	[33]
Foy 2.1, Foy 3.2, HIMT, Rom/Mn, Rom/Sb	19	Boschetti et al. (2022)	[34]
Jalame (with Mn)	6	Brill (1988)	[35]
HIMT, Foy 2.1, Foy 3.2	24	Bugoi et al. (2021)	[13]
Rom/Mn, Rom/Sb	7	Bugoi et al. (2022)	[36]
Egypt 1, HIMT a, HIMT b, HIT, HLIMT, Lev 1	168	Ceglia et al. (2015)	[37]
Fe-rich 6th cen	29	Cholakova et al. (2016)	[38]
HIT	3	Conte et al. (2014)	[39]
Egypt II, HIMT, Rom/Sb	21	De Juan Ares et al. (2017)	[40]
Foy 2.1, high Fe Foy 2.1	62	De Juan Ares et al. (2019)	[41]
HIMT	51	De Juan Ares et al. (2019)	[42]
Blue green, HIMT 1, HIMT 2, Levantine 1a, Levantine 1b	376	Foster et al. (2009)	[43]
Foy 2.1, Foy 3.1, Foy 3.1 (non tardifs), Foy 3.2, Foy 3.2 (non tardifs), Foy 3.3, Groupe 1	144	Foy et al. (2003)	[44]
RGBY1, RGBY2	12	Gliozzo et al. (2013)	[45]
Foy 3.2, HIMT, HIT, Lev 1, Mn decolorized, Sb decolorized	54	Maltoni et al. (2016)	[46]
Bet Eli'ezer, Egypt I, Egypt II	74	Phelps et al. (2016)	[47]
Fe rich Foy 2	31	Schibille et al. (2016)	[48]
Egypt 1A, Egypt 1B, Egypt 2 (high Na2O), Egypt 2 (low Na2O)	113	Schibille et al. (2019)	[49]
Ic1a, Ic1b, Ic2a, Ic2b	61	Silvestri (2008)	[50]
CL1, CL2	72	Silvestri et al. (2008)	[51]
	= 1538 samples	**= 24 publications**	

3.4.2 Novelty Detection with OCSVM

First novel glass types had to be identified. The reference database built from the literature data was building the foundation for the OCSVM. The scikit-learn library was used to train the model. The data was split into test- and train datasets, 100 randomly generated datapoints and 16 late-medieval natron glasses [52] were used as outliers for the training. All of the data was scaled. The tuning of the hyperparameter ν was achieved by evaluating the model by its error. The RBF-kernel was used, ν was set to 0.01 and γ was automatically chosen by the algorithm.

3.4.3 k-NN Model

Two k-NN models were employed in this study. One model, in the future referred to as k-NN model P, was trained to classify the raw materials' provenance, meaning the primary workshop. The other model, from now on named k-NN model GT, was designed to assign the unknown samples to the established glass types. The training of these models was conducted using the scikit-learn library. The collected database was subsequently divided into separate training and testing datasets, which were then scaled for further analysis. By cross-validation the optimal k-value was chosen.

3.4.4 Hierarchical Cluster Analysis (HCA)

In order to utilize all of the obtained analysis data gathered from LIBS and LA-ICP-MS the samples were clustered by themselves, without comparison to the publication data. Decoloring and Coloring agents were excluded to prevent clustering based on color. The scikit-learn library was used to scale the data and generate the dendrogram of the HCA.

3.4.5 Principal Component Analysis (PCA)

To visualize and aid in interpreting the results, a PCA was conducted on the samples, incorporating all measured element concentrations as features. The scikit-learn library was utilized once again to scale the data and conduct the PCA.

4 Results and Discussion

4.1 Elemental Analysis

Out of the 46 glass samples, which were analyzed in this work by Tandem-LIBS-LA-ICP-MS, 35 samples were also digested and measured with conventional liquid ICP-OES and -MS. All of the results can be found in separate tables in the *Appendix.* In this chapter the results of these measurements will be compared, to ensure the quality of the obtained data from the Tandem-LIBS-LA-ICP-MS measurements and the different quantification methods used.

In the analysis of liquid samples using ICP-OES, RSDs for major elements such as Al, Ca, Fe, K, Na, and Ti were consistently in the range of 1-2%. Minor components, including Ba, Sr, Mg, Mn, and Zr, also displayed favorable RSDs at approximately 1-2%. Notably, a significant improvement in RSDs was observed for certain trace elements, such as Cu, S, and Y, with RSDs ranging from 6-16% when subjected to a 1 to 10 dilution compared to a 1 to 100 dilution. However, some elements still exhibited higher RSDs, with La at 30%, P at 40%, and Sb at 100%. The method's Limits of Detection (LODs) were within the lower µg/g range. Furthermore, the analysis of liquid samples using ICP-MS yielded RSDs of approximately 1-3% for trace elements like Bi, Ce, Pr, Nd, Sn, and Pb. Ag and Cd exhibited RSDs of about 10%, while Gd had a 5% RSD. The LODs for liquid ICP-MS were in the lower ng/g range. Notably, when measuring certain trace elements, including Pr, Ce, Sn, and Pb, using ICP-OES, their RSDs were exceptionally high, exceeding 400%, despite the results being above the LOD. This led to a clear need for additional measurements with ICP-MS, which proved to be a productive approach.

Shifting our focus to solid measurements conducted with Tandem-LIBS-LA-ICP-MS, the results can be divided into two distinct segments; In the LIBS measurement major components like Ca and Na, showed RSDs around 2%, Si exhibited RSDs of 1-2%, and Al had an RSD of approximately 5%. Some minor components, such as Fe (7-10%), Ba, and Ti (20%), showed larger RSDs, while K had RSDs of around 8-10%. Conversely, minor components Mg and Mn displayed better RSDs, around 3%. In the case of LA-ICP-MS, RSDs for major components Si and Ca were very low, less than 1%, and Al had an RSD of 5%. Minor components Fe, Mn, and K showed RSDs of about 10%. Most trace elements exhibited RSDs of approximately 9-13%, with Cd and S having RSDs around 20%. Bi had an RSD of 30%, Ag and Li about 40%, and Au had the largest RSD at about 90%.

For solid measurements, it was not possible to determine the LOD because of the lack of a measurable blank when conducting direct solid sampling, and the use of a one-point calibration. Nevertheless, for most elements a low background signal was observed, which is a critical factor for ensuring a sensitive measurement. In general, LODs in LA-ICP-MS ranged

from ng/g to µg/g, depending on the analyte, while in LIBS, they typically fell in the mid to low µg/g range, also dependent on the specific analyte. [53], [54]

In conclusion, it is evident that the liquid measurements generally exhibited lower RSDs compared to the solid measurements, as expected. The higher RSDs for solid measurements are not necessarily measurement-related, but can also be connected to the higher inhomogeneity present in solid samples, when compared to liquid samples, which will be discussed in detail in the following chapter. However, it is worth noting that both major and minor components in the glass analysis still yielded satisfactory RSD results. LODs are much higher for the solid measurements, nevertheless still satisfactory for this particular application, which will be discussed later on in this work. To illustrate the divergence in results obtained through the different methods, refer to Figure 4.1 below, where pie charts depict the major and minor constituents of a representative sample measured using the three distinct methods.

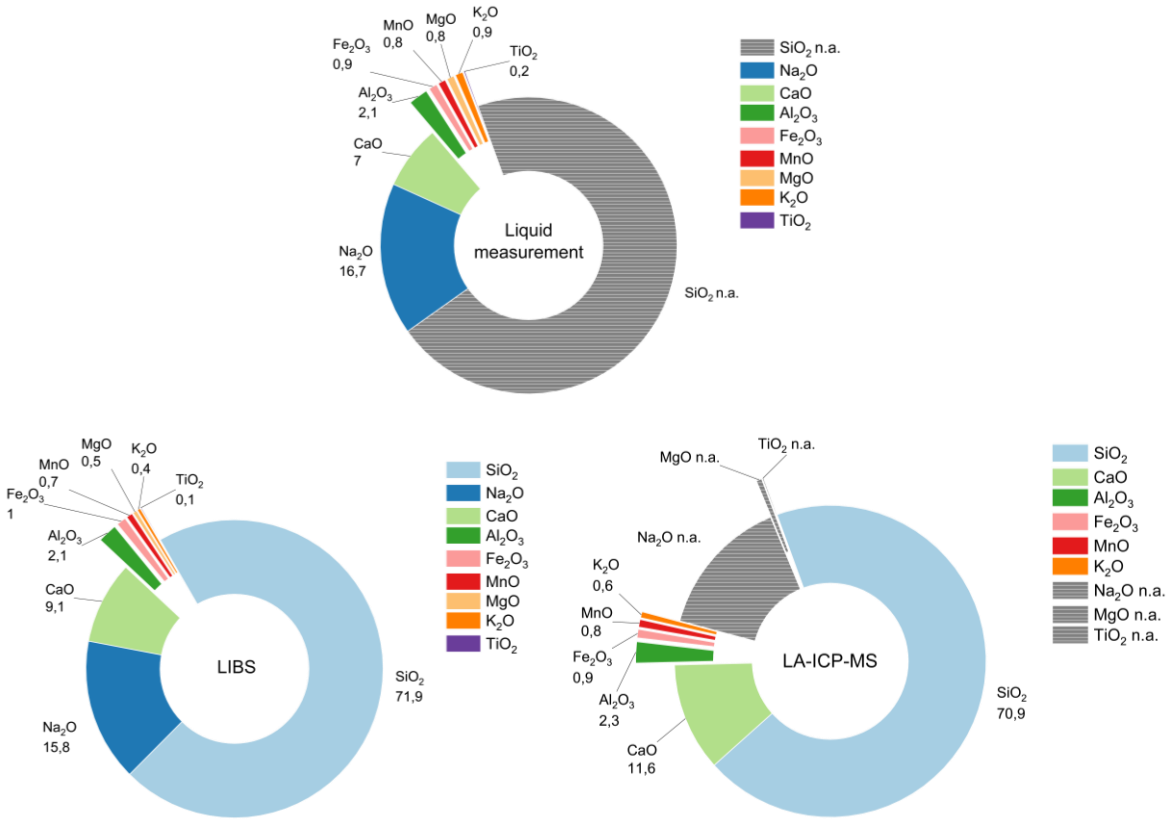

Figure 4.1: Comparison of the results for the different measurement methods for sample 5; values are listed in wt%

Overall, the results appear to align with each other. There are some variations in the Ca measurements between solid and liquid samples. One potential explanation for the variation in Ca results from liquid measurements could be the use of HF during the digestion process, which can form poorly soluble CaF_2. While CaF_2 precipitate should have been diluted with HCl, it remains a possibility to consider. Taking into account the potential interferences of Ca in ICP-MS measurements, as will be elaborated upon later in this study, there is also the possibility of consistent excess detection of the element in the ICP-MS results. It's important to emphasize that this figure also underscores the advantages of combining the two methods, LIBS and LA-ICP-MS. This combination allows for the measurement of major and minor components with LIBS, while LA-ICP-MS excels at detecting trace elements. Furthermore, the solid measurement in general enables the convenient and accurate measurement of Si. Further discussion on the disparities in solid measurements will be provided later.

Having addressed the comparison of the measurements, we will now delve into a detailed explanation of the quantification process with the solid measurements. To assess the differences between the measurement results, the deviation from solid to liquid measurement for each element and quantification method was calculated. The Mean Deviation (MD) was calculated for the 35 digested samples. Figure 4.2 illustrates the results for the sum normalization method used in LIBS, showing the different variants using different element lines of the LIBS spectra (see Table 3.5). Variant 5, together with drift correction (dc), yielded the most accurate results with the lowest overall MD.

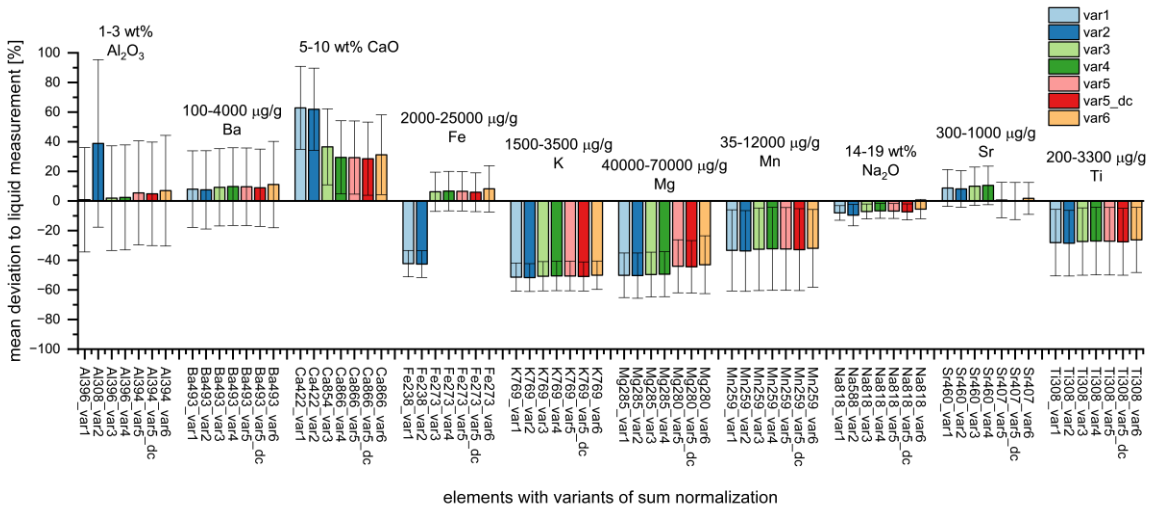

Figure 4.2: Comparison of the different variants of the sum normalization method for quantification with LIBS together with the approximate concentration range within the samples measured by LIBS

Afterwards, the semi-quantitative quantification method for LIBS without the sum normalization and the quantification results for the MS were evaluated and compared to the optimal variant of sum normalization, variant 5 with drift correction. This comparison can be seen in the following Figure 4.3. When comparing the quantification for LIBS with and without sum normalization, one can see, that even though for Al, Ba and Fe, the semi-quantitative method shows a better MD by a few percentage points, using sum normalization improved the accuracy for quantifying the elements K, Mg, Mn, Na, Sr and Ti.

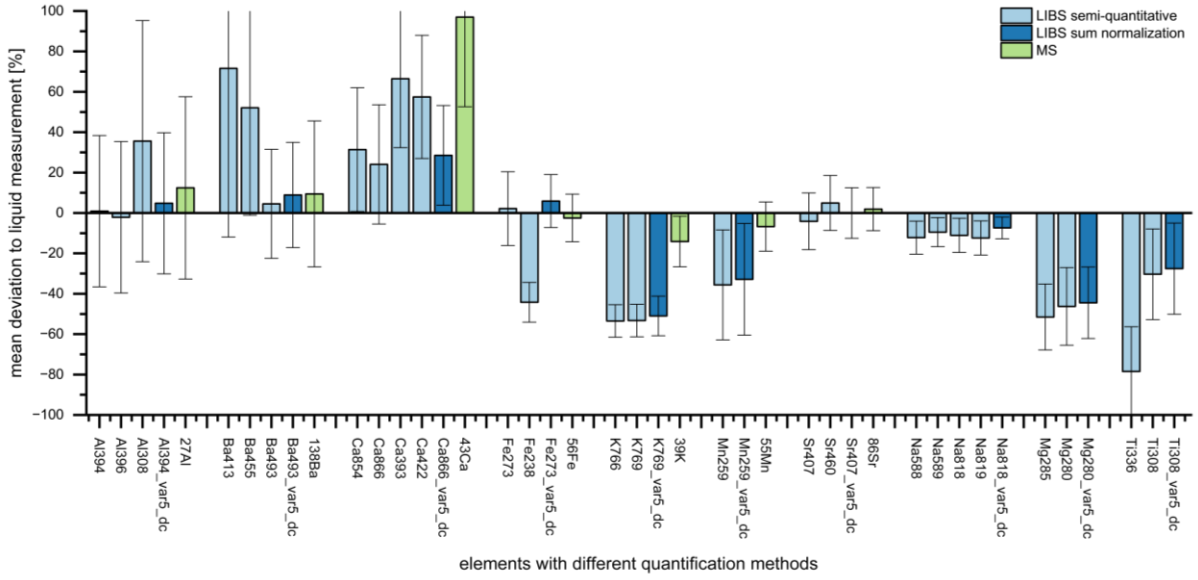

Figure 4.3: Comparison of different quantification methods

Notably, the LIBS data exhibited significantly higher precision for Ca compared to MS, with an MD of approximately 30 %, whereas the MS data displayed a much higher MD of around 100 %. Similarly, for Al, LIBS outperformed MS, achieving an MD of about 5 % compared to 12 % for MS. However, for other minor components such as K, Fe and Mn, MS provided better results. In the case of Sr and Ba, both methods yielded equally satisfactory outcomes. The elements Mg, Na and Ti were solely analyzed by LIBS, resulting in MDs of about 40 %, 10 % and 25 % respectively.

The trace elements, which were exclusively analyzed by LA-ICP-MS, showed significantly varied MDs. Those exceeding 40 % were excluded in the further statistical analysis, which applied for the elements Au, Bi, Co, Gd, La, Sc, P, Y and Yb.

In order to further underline the differences between the two solid measurements, the MDs of LIBS to LA-ICP-MS were calculated and plotted in Figure 4.4. Calcium shows the largest

discrepancy. When examining Ca using ICP-MS, numerous interferences can occur. The most abundant isotope $^{40}Ca^{+}$ cannot be measured because of the interference from $^{40}Ar^{+}$. Additionally, the other isotopes (^{42}Ca, ^{43}Ca, ^{44}Ca) show interferences with the oxides of other major and minor components of glass, such as Si, Al, Sr and Mg. [55] Whereas in the LIBS spectrum Ca shows multiple emission lines, which do not overlap with other element lines, making it easier to quantify it. Because Si could not be measured after the liquid digestion, as it forms volatile SiF_4, which evaporates during the evaporation, it was crucial to have satisfying results when comparing the two solid measurements. With an MD approaching zero this could be achieved.

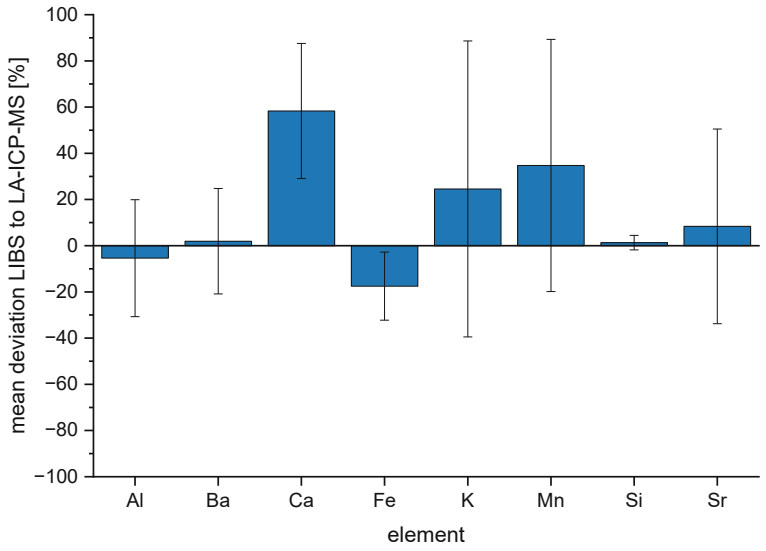

Figure 4.4: Comparison of LIBS and LA-ICP-MS

In the following Table 4.1 an overview over combined results from LIBS for the major and minor components and LA-ICP-MS for the trace elements can be found, listing the concentration ranges, means and Relative Standard Deviations (RSDs) of the measured components, which will now be used to further discuss the quantification results.

The underlying cause for the challenges encountered by LIBS in quantifying Fe, K, Mn and also Mg (see Figure 4.3) could be the chosen reference material NIST® SRM® 610. While the concentration ranges of these elements, as to be seen in Table 4.1, are rather large, they also exceed the concentrations in the reference material by far, which lie around 500 µg/g for the minor components and trace elements of the samples. Using reference materials, which better fit the composition of historical glass, such as the Corning Reference Glasses, this error could probably be minimized.

Table 4.1: Combined results from LIBS and LA-ICP-MS measurement: concentration range, mean and RSD

		Minimum	*Maximum*	*Mean*	*RSD [%]*
Concentration measured with LIBS [wt%]	*SiO_2*	67	72	70	1.9
	Na_2O	14	*19*	*17*	*7.4*
	CaO	5.3	10	7.7	16
	Fe_2O_3	0.3	3.7	1.4	60
	Al_2O_3	1.4	2.7	2.1	15
	MnO	0.0045	1.6	0.8	44
	MgO	0.24	0.56	0.45	18
	TiO_2	0.032	0.55	0.19	86
	BaO	0.014	0.45	0.054	150
	K_2O	0.19	0.43	0.29	23
	SrO	0.035	0.11	0.066	26
Concentration measured with LA-ICP-MS [µg/g]	Sb	0.28	3900	220	290
	Pb	4.6	3200	200	250
	Co	0.85	2200	99	370
	S	710	2100	1400	27
	Cu	4.3	1800	190	210
	P	270	640	410	24
	Zr	21	200	77	66
	Sn	0.3	100	13	180
	Zn	11	90	32	47
	Ce	8.8	21	14	22
	Ce	6.2	18	10	26
	Y	5.3	17	9	27
	La	5	17	8.6	29
	Nd	4.4	15	7.5	30
	Li	2.8	12	6.1	35
	Cd	0.066	11	1.3	170
	Sc	2.3	8.4	4.6	38
	Pr	1.2	4.1	2	30
	Gd	0.98	3.5	1.7	31
	Yb	0.45	1.7	0.89	33
	Ag	0.011	1.1	0.13	170
	Bi	0.0059	0.18	0.038	93
	Au	0.0022	0.097	0.014	130

Nevertheless, the concentration range is in general rather large, as well as the variation of the compositions expressed by the RSDs, implying that the MD should not have significant impact

on the classification of the glass. Therefore, for further statistical analysis, the results of the major and minor components of the samples were extracted from the LIBS data and combined with the trace element results, analyzed by LA-ICP-MS, as seen in Table 4.1. This decision was made to highlight the potential advantage that LIBS could offer if included in the analysis. The detailed combined data used for statistical analysis can be found in the *Appendix*. The RSDs of the 46 samples measured with Tandem-LIBS-LA-ICP-MS are visualized in Figure 4.5 and will also be furtherly discussed in following chapters. High RSDs, such as those observed for Fe or Sb, highlight the wide range of compositions within the sample set. On the other hand, Si concentrations remain remarkably consistent across all samples, leading to a low RSD.

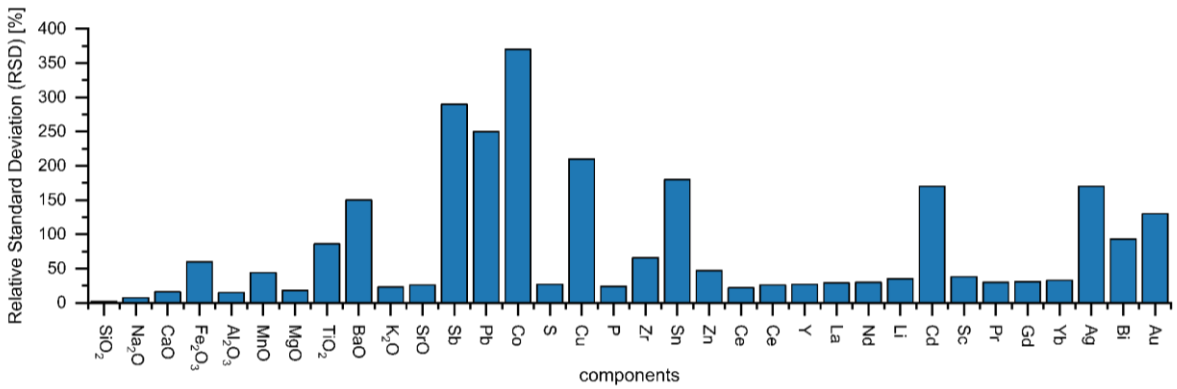

Figure 4.5: Relative Standard Deviations (RSDs) for the different components of the glass samples, depicting the variation of the samples' compositions

4.1.1 Investigation of Homogeneity

In antiquity, during the production of glass, the raw materials were melted over extended periods, ranging from hours to days. This prolonged melting process homogenized the material thoroughly, resulting in a material that is highly suitable for direct solid sampling, because of its high probability to be highly homogeneous. When using direct solid sampling the homogeneity of the analyzed material is crucial. That is why three samples were randomly chosen to undergo a full imaging with LIBS. The measurement conditions can be found in the chapter *Measurement with Tandem-LIBS-LA-ICP-MS*. The results for sample 4, together with an image of the original artifact and the microscopic image of the embedded sample fragment, can be seen in the following Figure 4.6. In the imaging results seen on the right hand side of the figure, the signal intensity for different elements is visualized.

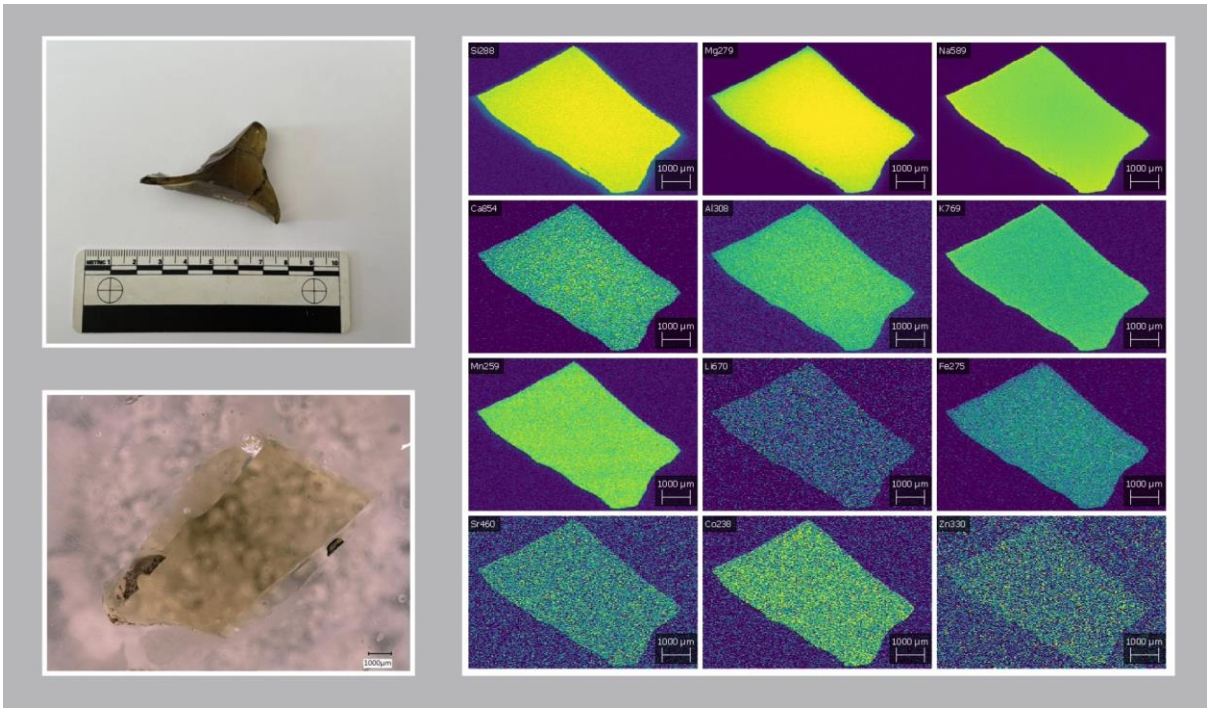

Figure 4.6: Imaging results using LIBS for sample 4;
top left: original artifact of sample
bottom left: microscopic image of embedded sample
right: imaging results with distribution of major and minor components and trace elements

By utilizing the iolite software and selecting the area of interest, the RSDs of the signal intensity within the area of the specimen can be computed. As an illustration of the homogeneity of the material, the table below displays the RSD of the signal intensity for a major component (Si), a minor component (Mg), and a trace element (Co). Although the RSD varies between different samples and elements, it consistently remains below 5% for all cases.

Table 4.2: RSD of signal intensity for three elements and concentrations

		Sample 4	*Sample 25*	*Sample 40*
Si (Major component)	|RSD| of signal intensity [%]	2.2	4.8	0.1
	concentration [µg/g]	323693	323843	319813
Mg (Minor component)	|RSD| of signal intensity [%]	2.3	3.3	0.1
	concentration [µg/g]	3298	2885	3166
Co (Trace element)	|RSD| of signal intensity [%]	0.6	2.6	0.9
	concentration [µg/g]	8	6	20

The optical proof, together with the low RSDs, confirm the suspected homogeneity of the material, making it suitable for direct solid sampling. The imaging results for sample 40 and 25 can be found in the *Appendix* and furtherly confirm the outcome of this investigation.

4.1.2 Assignment to Major Glass Group

Before the statistical analysis, the initial evaluation of the data focused on identifying the major glass group had to take place. As previously mentioned, Late Antiquity could have included not only natron glasses but also plant ash glasses. To differentiate between the two, a plot of MgO against K_2O was performed using data obtained through LIBS. This analysis conclusively demonstrated that none of the samples met the established literature threshold of 1.5 wt% for plant ash glasses, discussed before in the chapter *The Investigated Material from an Archaeometric Perspective,* definitively classifying the glasses as natron glasses. [1]

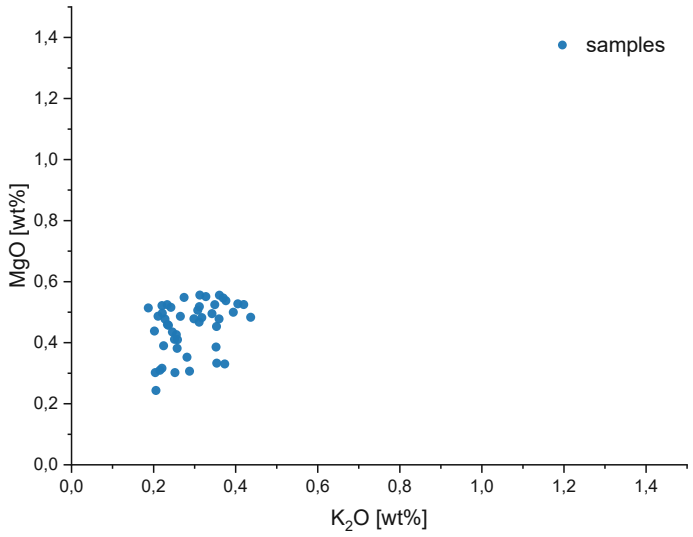

Figure 4.7: Assignment to Natron glass by MgO- and K_2O content

4.2 Statistical Analysis

Generally, when discussing the identification of new types of glasses that have not been documented in existing literature, and their categorization into established glass types, a challenge arises when there is a lack of prior knowledge and no glass types can be excluded in advance. In such cases, traditional visual and manual assignment methods, as demonstrated in previous studies (e.g. [29], [56]), become impractical. The complexity of the data increases with the sheer volume of data points, leading to overlapping data clouds in various biplots of major and minor components and also in PCA. Therefore, to tackle this problem effectively, the suitable approach involves employing one or more algorithms that consider all features simultaneously, eliminating the need for visual assistance in assigning groups.

The chapter *Experimental* introduced Figure 3.8, which displays a useful overview over the statistical method used and depicts a useful reference for the following subchapters.

4.2.1 Recycling Markers and Decoloring Agents

Elements associated with coloring of historical glasses are Co, Ni, Cu, Zn, As, Se, Ag, Cd, In, Sn, Au, Hg and Pb. If one of the chromophores is present in a concentration range between 100 and 1000 µg/g the sample is believed to be recycled, and the trace elements, the Recycling markers (RM), were introduced into the glass batch by adding e.g. deliberately colored glass to colorless glass. Also, if the Decoloring agents (DA) Mn and Sb are present in the sample simultaneously with a concentration of more than 100 µg/g it is most likely also recycled, as explained before in the chapter *Theoretical Background* [12]. While Ceglia et al. introduced a new approach to RM in 2019 [57] with more precise thresholds for different elements, the common approach of a larger threshold of 100 µg/g was chosen, as described by Brems et al. [12]. The reason for this choice is the necessity to know the glass group to establish specific thresholds. Ceglia et al. focused mainly on defining definite thresholds for Levantine 1, whereas the thresholds for Egyptian HIMT glasses were kept very general due to the absence of raw glass from the furnaces, which is essential for defining the unrecycled glass type. Since this work approached the analysis without prior knowledge, larger thresholds were retained to maintain generalization, considering that the glass groups might differ from those for which the RM were defined. Additionally, it should be noted that these thresholds are somewhat arbitrary, and additional information about the investigated artifact could provide more insights into the recycling question.

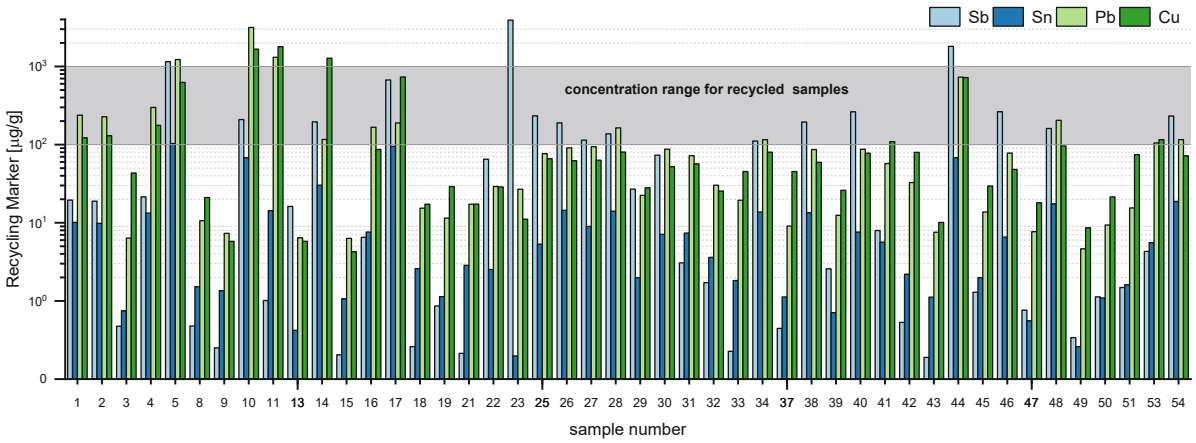

Figure 4.8: Recycling Markers detected by LA-ICP-MS with marked area for recycled samples

After assigning the samples to the group of Natron glasses the RM and DA were analyzed, to exclude recycled samples beforehand. In Figure 4.8 the RM Sb, Sn, Pb and Cu, which could be detected and successfully quantified with LA-ICP-MS, are shown. The area of the concentration range for recycled samples is marked in dark grey. Furthermore, the two DAs, Sb and Mn, are displayed together in Figure 4.9, as their simultaneous occurrence with a cut-off value of 100 µg/g (see red line in figure) also implies recycling.

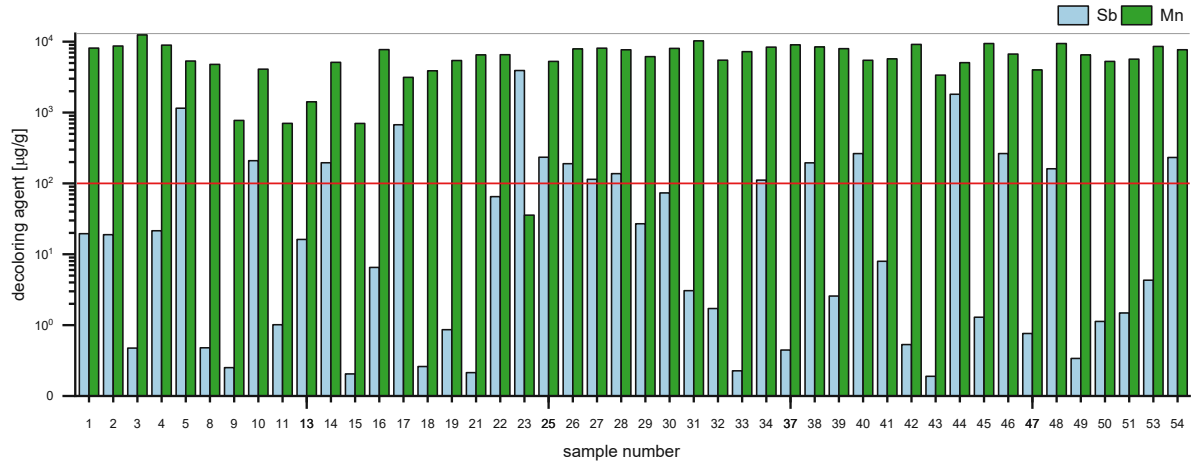

Figure 4.9: Decoloring Agents detected by LA-ICP-MS with the cut-off value of 100 µg/g marked in red

Three samples, samples 10, 11 and 14, will be discussed in detail due to their distinct feature of exhibiting a deep blue color. Even though the measured concentrations for Co were not included in the statistical evaluation due to the high MD of about 80 %, they still revealed a significant finding. In these three samples 10, 11 and 14 the concentration of Co was

approximately 100 times greater than in the other samples, as they showed Co contents of 2170, 1200 and 750 µg/g respectively, while the other samples displayed only minimal Co content in the range of a few µg/g. This data suggests strongly that Co was the colorant responsible for achieving the deep blue hue. The high variation of the Co contents in the samples in comparison to the other components is highlighted by Figure 4.5, showing the notably high RSD of Co contents. With that knowledge, sample 10 and 14 can be excluded from the list of recycled samples, because their elevated Cu, Pb and Sn values are probably caused by the Co source used in the glass batch. [58]

In conclusion the analysis revealed the following results: 27 samples showed no RM or both DAs whatsoever, 4 colorless or naturally colored samples showed elevated RM, and 15 samples contained both DAs. With the deep blue samples excluded this concludes to 17 samples which are most likely recycled glass. The detailed assignment will be listed in following chapters.

4.2.2 Novelty Detection with OCSVM

Before utilizing the quantification results of the samples in a classification model, it is crucial to assess whether the base elemental composition of the unrecycled glasses, specifically SiO_2, Na_2O, CaO, Fe_2O_3, Al_2O_3, MnO, MgO, TiO_2 and K_2O (see Table 4.1) falls within the ranges of the base composition of the samples in the reference database extracted from the literature. To rightfully interpretate the classification results, novelties, that fall out of the data structure of the reference dataset, must be detected.

To accomplish that an OCSVM model was trained with the reference dataset, using the 9 minor and major components as features, to establish a boundary between known and novel glasses and applied to the samples. During the training phase, the hyperparameter v was fine-tuned by comparing the model's error. The outcomes are presented in Table 4.3, which clearly demonstrates that a value of 0.01 for v resulted in the lowest error. Therefore, this value was selected for the final model. The final model was applied to the unknown samples, using the analysis data obtained by LIBS.

Table 4.3: Tuning of hyperparameter

	v = 0.001	**v = 0.01**	**v = 0.1**
Relative error train [%]	2.44	2.20	10.26
Relative error test [%]	4.89	4.89	11.73
Relative error random outliers [%]	0	0	0
Relative error late-medieval glass [%]	0	0	0

The biplots typically used for the assignment to a glass type in the literature have been used to visualize the results of the detection of novel glass types with OCSVM, as a visualization of the OCSVM results with the trained boundary cannot be done when having more than two features. The resulting scatter matrix can be seen in Figure 4.10, which not only presents the results but also explains the problematic with a visual assignment discussed beforehand.

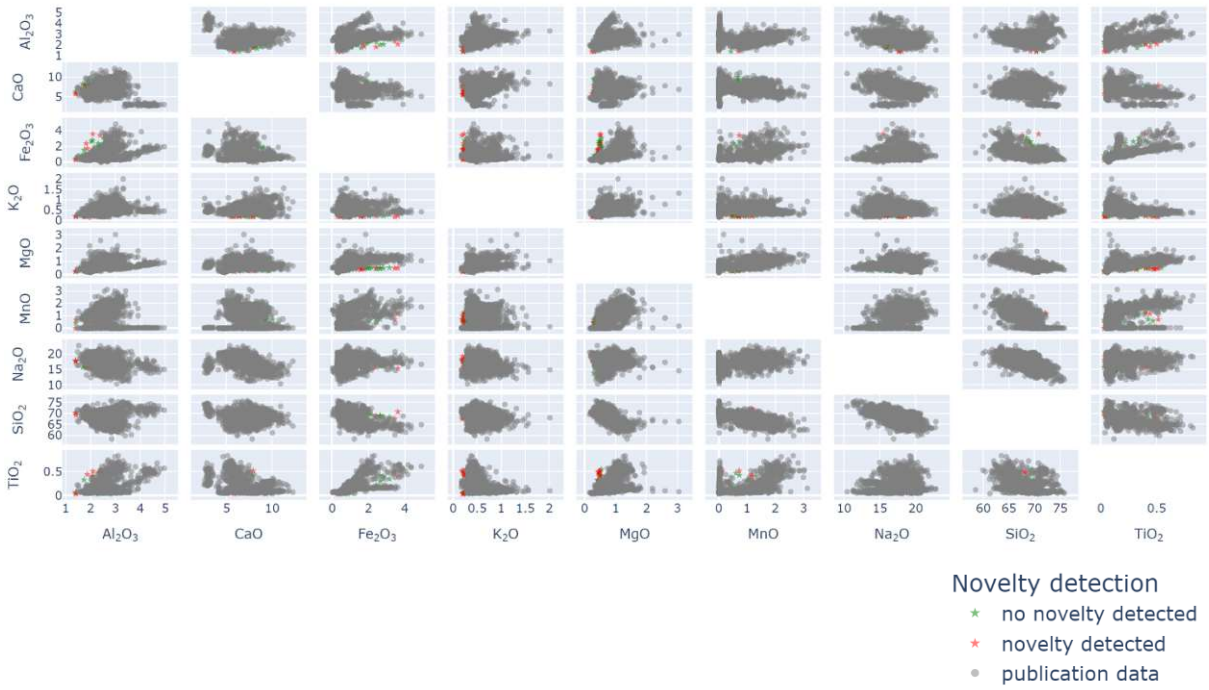

Figure 4.10: Scatter matrix of the results of the OCSVM for novelty detection

Out of the total analyzed glass samples, 15 were identified as novel glass types, while the remaining 31 appeared to have a base composition similar to the established glass types. The detailed assignment will be listed in following chapters, as well as the discussion of the elemental compositions of the novel glasses.

It is essential to clarify that the term "novel glass types" in this work refers specifically to glasses that are not documented in the literature included within the database, the constituents of which is listed in the chapter *Experimental*. Additionally, this classification is solely reliant on the analysis of the major and minor components of the glass. This choice of major and minor components for analysis was made based on the least common multiple found in the literature data, to include as much data as possible. Furthermore, one must keep in mind that this novel glass composition can also result from a mixing of different glass types due to recycling, but this will be addressed later on in this work.

4.2.3 Clustering of the Samples with HCA

In order to integrate all the acquired data effectively, a HCA was conducted on the combined data set comprising major and minor components and trace elements, meaning the data obtained by LIBS and LA-ICP-MS. The purpose of the HCA results is to aid in interpreting the combined statistical evaluations by having the samples grouped accordingly. These findings will be further discussed in subsequent sections of this work.

4.2.4 k-NN Classification for Distinguishing Primary Location and Glass Type

After identifying recycled and novel samples, two k-NN algorithms were trained, using the reference dataset, and applied to the unknown samples. This classification relied solely on the analysis data obtained by LIBS, as discussed in the chapter *Elemental Analysis.* The k-NN-classification occurred in two stages: First, the samples were classified into the two primary workshop locations: Egypt or Levant (k-NN P). Then, a second classification was performed to identify different glass types (k-NN GT).

Determining the optimal value of k for the model necessitates cross-validation. To achieve this, each k value was tested, and the corresponding model accuracy was plotted, as illustrated below. The plots show the results of the cross-validation, revealing that the optimal k value for the k-NN model GT is 6 and 2 for the k-NN model P. These particular k values maximize the accuracy of the respective models.

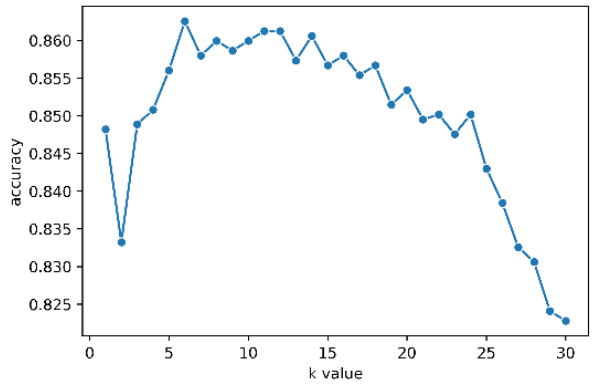

Figure 4.11: Cross-validation for k-NN model GT

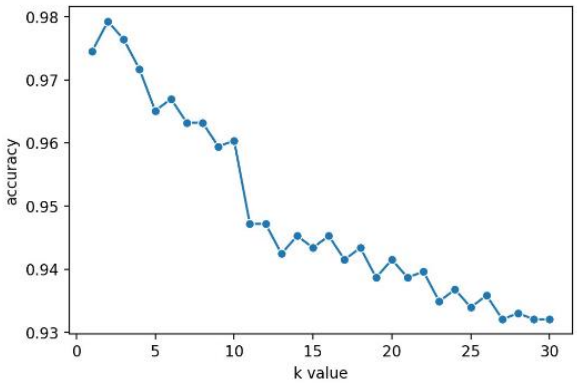

Figure 4.12: Cross-validation for k-NN model P

During the training of the k-NN model GT, it was observed that utilizing all the distinct glass groups listed in Table 3.9 resulted in a relatively low accuracy rate of approximately 70 %. Upon inspecting the confusion matrices, it became evident that numerous established glass types showed significant similarities to one another. Based on the information gleaned from

the confusion matrices and corroborating literature, the author made the decision to combine the smaller groups to larger ones. This step was taken because the literature confirmed that certain glass types, although historically labeled differently, are, in fact, identical and by the combination the performance of the model could be enhanced. The confusion matrix of the final model with the combined groups with an accuracy of approximately 90 % can be seen below in Figure 4.13.

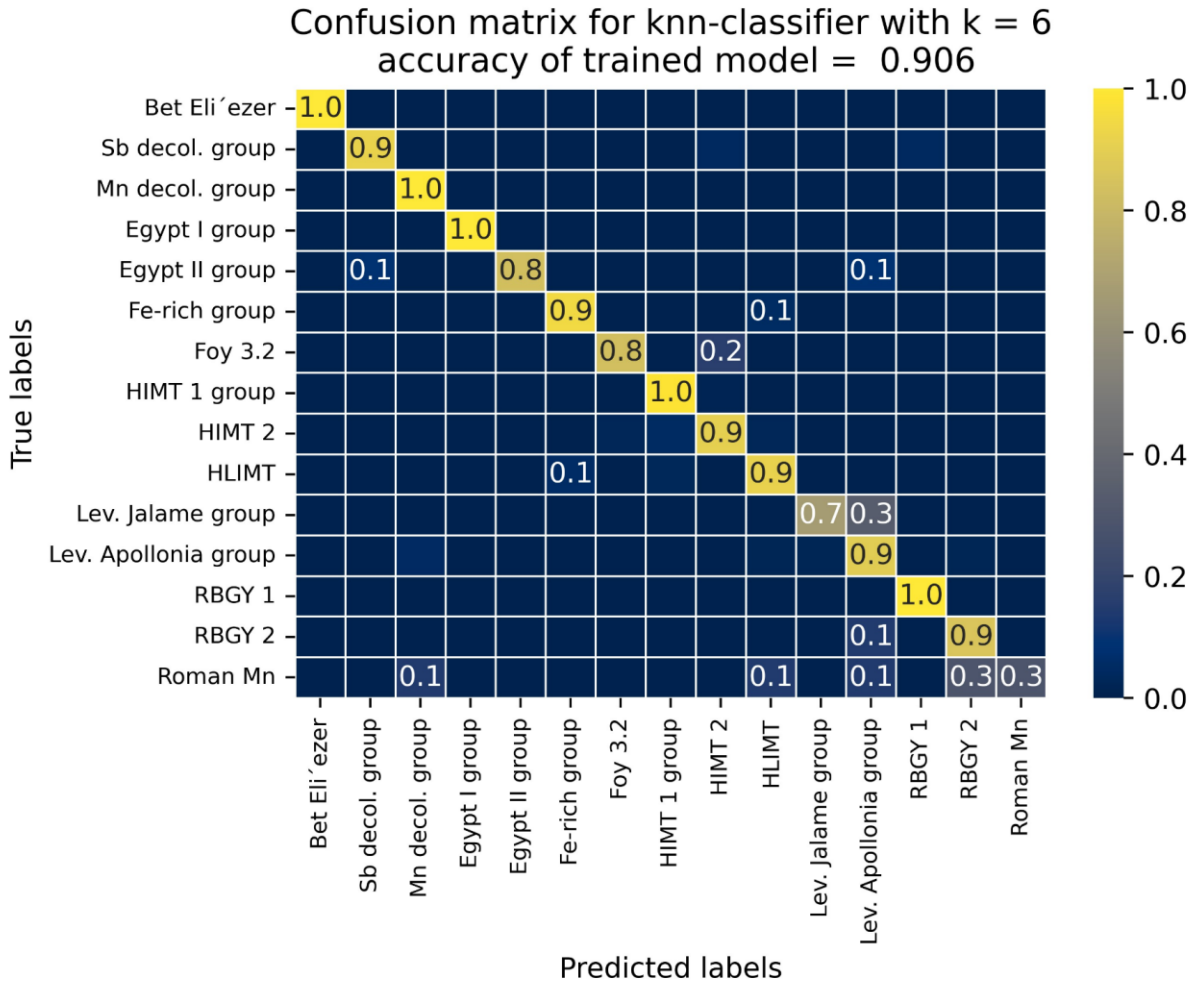

Figure 4.13: Confusion matrix of the k-NN model GT

The following Table 4.4 contains the abbreviated class names and the corresponding groups they represent and can be seen below. For the connection of the groups to literature refer to Table 3.9.

Table 4.4: Class name abbreviations

abbreviated class names	*full class names*
Bet Eli'ezer	Bet Eli'ezer
Sb decol. group	CL 1 / Roman Sb / Sb decolorized
Mn decol. group	CL 2 / Mn decolorized / Mn-a
Egypt I group	Egypt I / Egypt 1A / Egypt 1B
Egypt II group	Egypt II / Egypt 2 (high Na2O) / Egypt 2 (low Na2O)
Fe-rich group	Fe-rich: Foy 2.1, HLIMT, 6th cen
Foy 3.2	Foy 3.2 / Foy 3.2 (non tardifs)
HIMT 1 group	HIMT / HIMT a / HIMT b / HIMT 1 / Foy Groupe 1 / HIT
HIMT 2	HIMT 2
HLIMT	HLIMT / Foy 2.1 / Foy 2.2 / Foy 2
Lev. Jalame group	Lev - Jalame / Levantine B / Foy 3.3
Lev. Apollonia group	Lev 1 / Apollonia / Levantine A / Foy 3.1 / Foy 3.1 (non tardifs)
RBGY 1	RBGY1 / Ic1a / Ic1b
RBGY 2	RBGY2 / Ic2a / Ic2b
Roman Mn	Roman Mn

The resulting performances of the two k-NN-models are displayed in Table 4.5, showing accuracy, precision and recall.

Table 4.5: Performance of k-NN models

	Accuracy [%]	*Precision [%]*	*Recall [%]*
k-NN GT (k = 6)	0.91	0.81	0.82
k-NN P (k = 2)	0.99	0.99	0.99

The resulting probabilities for the classes for each sample were visualized in pie charts and can be seen in Figure 4.14 and Figure 4.15. The charts provide a clear and intuitive representation of the models' outcomes, each slice of the pie representing a distinct provenance or glass type.

Figure 4.14 shows the results for the k-NN model P, differentiating the samples between glasses with its primary production workshop located in Egypt or Levant. While most samples were clearly attributed to a specific provenance, three samples exhibited nearly equal probabilities of belonging to both provenances. It's important to consider whether these samples are recycled or new glasses, a topic that will be explored in a later section of this chapter.

Figure 4.14: Resulting probability for classification of samples to primary workshop location (k-NN P)

Figure 4.15 displays the resulting probabilities for the assignment to the established glass types, collected in the reference database. Much like the outcomes observed in k-NN model P, a subset of samples did not receive exclusive classification under a single glass type.

Figure 4.15: Resulting probability for classification of samples to glass types (k-NN GT)

4.2.5 Combining the Results of the Statistical Assessment

After conducting these various evaluations, all the obtained results by the detection of the RM and DA, the novelty detection and the k-NN-models can be visualized in consolidated tables. These tables provide comprehensive overview over the analyzed samples and can lead to a conclusive statements regarding the provenance of the samples and its similarity to already found glass types. In the following the results will be divided into different sections for clarity.

In these consolidated tables also the results of the HCA are listed. It is evident that, to some extent, the HCA clusters the samples based on its color. Even though the chromophores were excluded from the list of features for the HCA, other trace components, which are not chromophores themselves, still guide the HCA in this particular direction. This must mean, that certain trace elements were introduced in the glass batch during the glass making process together with the coloring agents. The results of the HCA are still included in the results, because for some groups it shows similarities between the samples. For example HCA class 5 is found in all three subchapters, all of them including some type of HIMT glass.

4.2.5.1 Assignment to Established Glass Types

Nineteen glass samples were not detected as a novelty and did not show any RM or both DAs. Consequently, these samples can be straightforwardly classified into the in the literature established glass types. In certain instances, a single sample may be associated with more than one class. Table 4.6 below displays the joint results for these samples.

Table 4.6: Combined statistical evaluation for known glass types without Recycling markers cl = colorless, L = Levant, E = Egypt

#	Color	DA	RM	Novelty	k-NN GT class. result	k-NN P class. result	HCA
10	blue	Sb/Mn	(Yes)	No	Fe-rich group + HIMT 2	E	2
14	blue	Sb/Mn	(Yes)	No	Lev. Apollonia group	L	4
3	light yellow	Mn	No	No	HIMT 1 group	E	5
16	green	Mn	No	No	HIMT 1 group	E	5
51	light yellow	Mn	No	No	HIMT 1 group	E	5
8	light green	Mn	No	No	HIMT 1 group	E	5
31	light yellow	Mn	No	No	HIMT 1 group	E	5
21	cl	Mn	No	No	~~RBGY 2~~ + Lev. Apollonia group + Foy 3.2	L	6
30	cl	Mn	No	No	HLIMT + ~~RBGY2~~ + Roman Mn	L	6
32	cl	Mn	No	No	Roman Mn + Foy 3.2 + Lev. Apollonia group	L	6
39	green	Mn	No	No	HIMT 1 group + HIMT 2	E	7
45	green	Mn	No	No	HIMT 1 group + HIMT 2	E	7
13	light green	Mn	No	No	Lev. Apollonia group + Lev. Jalame group	L	8
22	cl	Mn	No	No	HIMT 2 + Foy 3.2	E	8

29	cl	Mn	No	No	HIMT 2 + ~~RBGY 1~~ + Lev. Apollonia group	E	8
43	cl	Mn	No	No	Sb decol. group	E	8
47	cl	Mn	No	No	Sb decol. group	E	8
49	cl	Mn	No	No	HIMT 2 + Foy 3.2	E	8
50	cl	Mn	No	No	HIMT 2 + Foy 3.2	E	8

For three samples it was possible to exclude classes due to their color. The colorless samples 30, 29 and 21 were assigned to the class “Roman Blue Green Yellow 2” (RBGY 2), which resembles only colorful glass. The resulting distribution of the classes and the samples’ provenance for these 19 samples can be seen in the pie chart in Figure 4.16. In total 14 samples are from Egypt, and 5 of them from Levant.

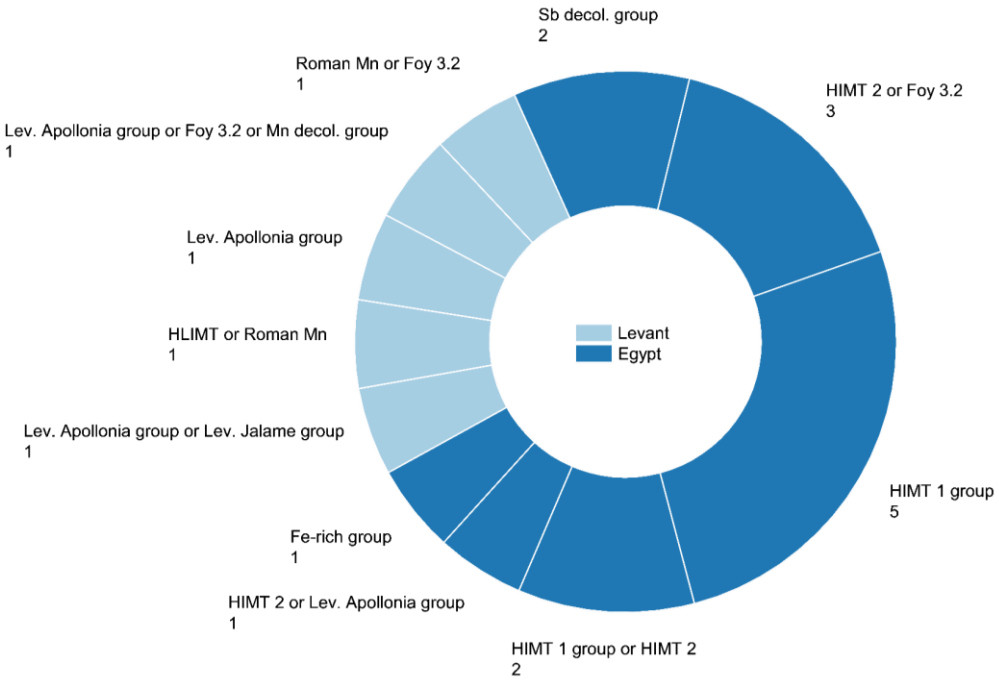

Figure 4.16: Overview of analyzed glass samples without Recycling markers

4.2.5.2 Recycled Glasses

The statistical evaluation of the seventeen glass samples, which are believed to be recycled, should be considered as more of a guiding indication. Since recycled glasses may consist of various mixed glass samples, the results can provide only an idea of what is potentially included in the mixture. Nevertheless, it can be utilized as an interpretation to gain insights

into the composition of the ancient glasses. In this case, no classes could be excluded based solely on color. Considering sample 44 as an example, despite being colorless, the k-NN algorithm indicates similarities of this glass sample to RBGY 1, besides the Levantine Apollonia group. The presence of elevated RMs and both Sb and Mn in the sample suggests that RBGY 1 might have been mixed into the batch along with Levantine Apollonia group-type glass during a recycling process. This blending of glass types could explain the observed characteristics in sample 44, despite its colorless appearance.

Table 4.7: Combined statistical evaluation for glass samples with Recycling markers
cl = colorless, L = Levant, E = Egypt

#	Color	DA	RM	k-NN GT class. result	k-NN P class. result	HCA
5	light green	Sb/Mn	Yes	Lev. Apollonia group + RBGY 2	L	3
44	cl	Sb/Mn	Yes	Lev. Apollonia group + RBGY 1	L	3
17	light green	Sb/Mn	Yes	Lev. Apollonia group	L	4
53	cl	Mn	Yes	HIMT 1 group + Fe-rich group	E	5
27	cl	Sb/Mn	Yes	HLIMT	E	6
34	cl	Sb/Mn	Yes	HLIMT	E	6
54	cl	Sb/Mn	Yes	HLIMT	E	6
46	light yellow	Sb/Mn	Yes	HLIMT + Fe-rich group	E/L	6
28	cl	Sb/Mn	Yes	HLIMT + RBGY 2	E/L	6
26	cl	Sb/Mn	Yes	HLIMT + Roman Mn	L	6
25	cl	Sb/Mn	Yes	Lev. Apollonia group + HLIMT + HIMT 2	L	6
38	cl	Sb/Mn	Yes	HLIMT	E	6
4	light yellow	Mn	Yes	HLIMT + Fe-rich group	E	6
2	light yellow	Mn	Yes	HLIMT + Fe-rich group + Egypt II group	E	6
1	light yellow	Mn	Yes	HLIMT + Fe-rich group + Egypt II group	E/L	6
48	cl	Sb/Mn	Yes	Lev. Apollonia group + Lev. Jalame group + HLIMT + Roman Mn	L	6
40	cl	Sb/Mn	Yes	Lev. Jalame group + HLIMT	L	6

As an alternative to the trace elements used in this study, authors have attempted the detection of recycling using more specific trace element thresholds [57] or isotopic signatures [59]. However, as mentioned before, these methods were not employed because the most definite glass would be needed to create a baseline for these thresholds.

The combined results of the recycled glass samples can be seen in the pie chart in Figure 4.17.

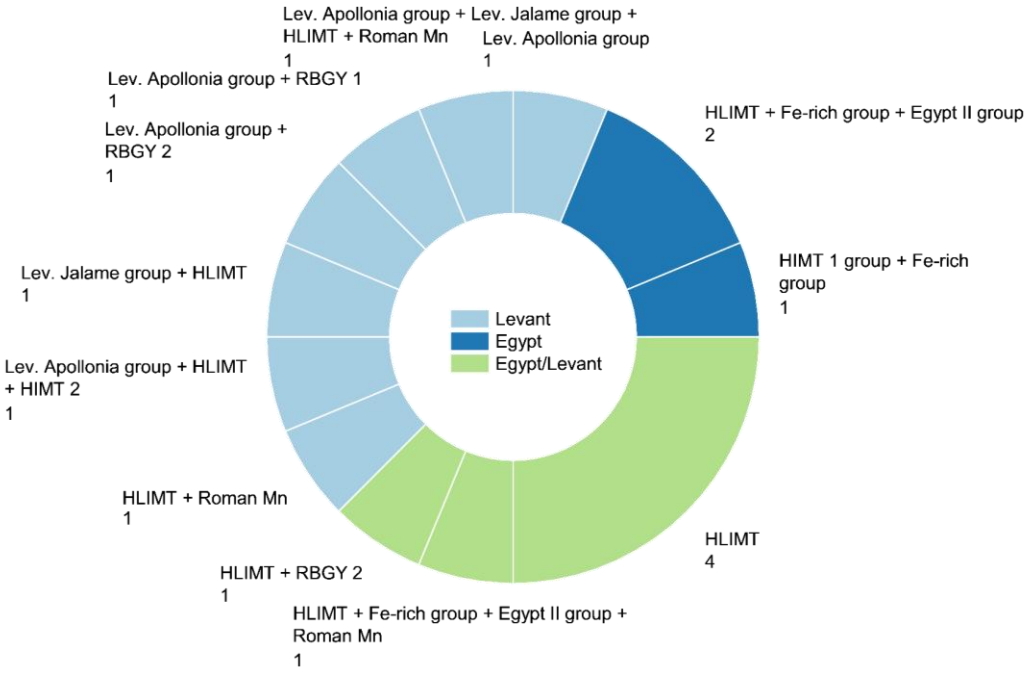

Figure 4.17: Overview of analyzed glass samples with Recycling markers

4.2.5.3 Novel Glass Types

A total of ten glass samples were detected as novelties and did not exhibit any RMs, meaning its deviation most likely does not come from the mixture with other glass types. For these samples, the classification cannot be taken literally, but rather serves as an indication of a similarity to an already established glass type.

Table 4.8: Combined statistical evaluation for glass samples detected as novelties
cl = colorless, L = Levant, E = Egypt

#	Color	DA	RM	Novelty	k-NN GT class. result	k-NN P class. result	HCA
23	cl	Sb	No	Yes	Sb decol. group	E	1
11	blue	Mn	No	Yes	HIMT 1 group + Egypt I group	E	2
9	light green	Mn	No	Yes	HIMT 1 group + Egypt I group	E	5
15	light green	Mn	No	Yes	HIMT 1 group + Egypt I group	E	5
33	cl	Mn	No	Yes	HIMT 1 group + HLIMT	E	5
37	cl	Mn	No	Yes	HIMT 1 group + HIMT 2	E	5

41	green	Mn	No	Yes	HIMT 1 group + Fe-rich group + HLIMT	E	5
42	cl	Mn	No	Yes	HIMT 1 group	E	5
18	cl	Mn	No	Yes	Sb decol. group + Foy 3.2 + HIMT 2	E	8
19	cl	Mn	No	Yes	Sb decol. group + Foy 3.2	E	8

The combined results are once again visualized in a pie chart seen below in Figure 4.18. All of these ten samples are of Egyptian origin, showing close resemblance to the HIMT 1 group, but also to the Sb decolorized group.

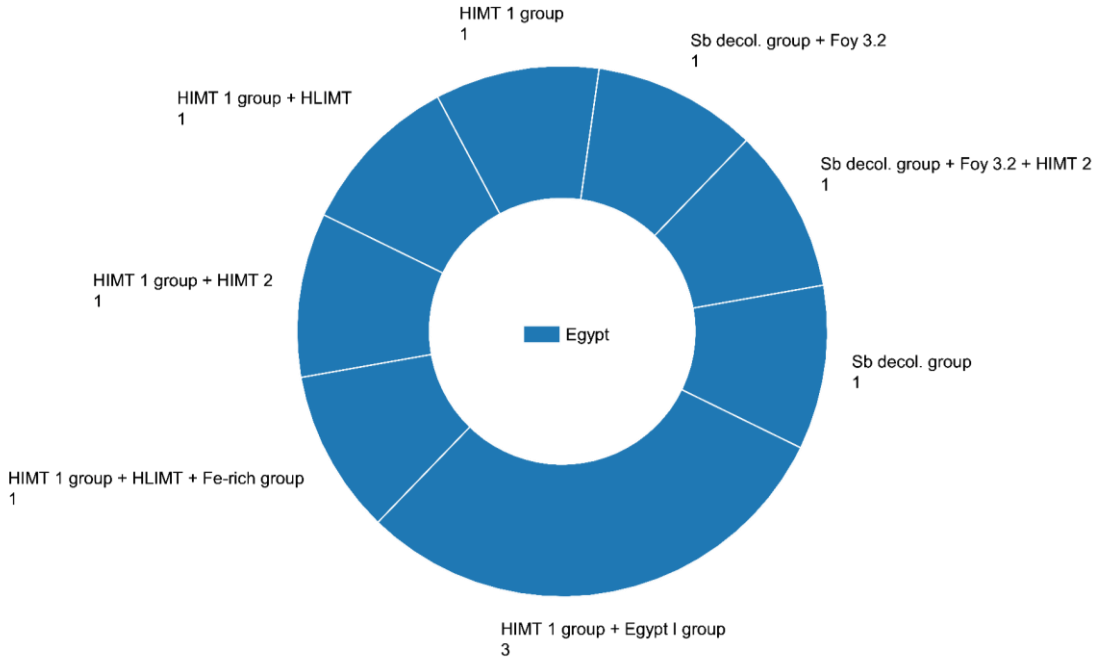

Figure 4.18: Overview of analyzed glass samples detected as novelties

4.2.6 Further Interpretation of the Elemental Analysis

With the primary workshop locations of the samples identified, we can now closely compare the compositions of the samples originating from Egypt and Levant. The mean values of every element concentration were calculated for each provenance group identified, still separated by the occurrence of RM and successful novelty detection. These mean values were then normalized and visualized on a heat map, which can be seen in Figure 4.19. The mean values and standard deviations, are shown in detail in Table 9.8 in the *Appendix*.

The heat map once again highlights the usefulness of an algorithm used in comparison to manual evaluation, as the algorithm can effectively assess all the given variables together, while a visual assignment for all the samples separately without having them grouped before by an algorithm seems rather impossible. Now that groups have been identified though, interpretation can be done more easily, which should be done in the following.

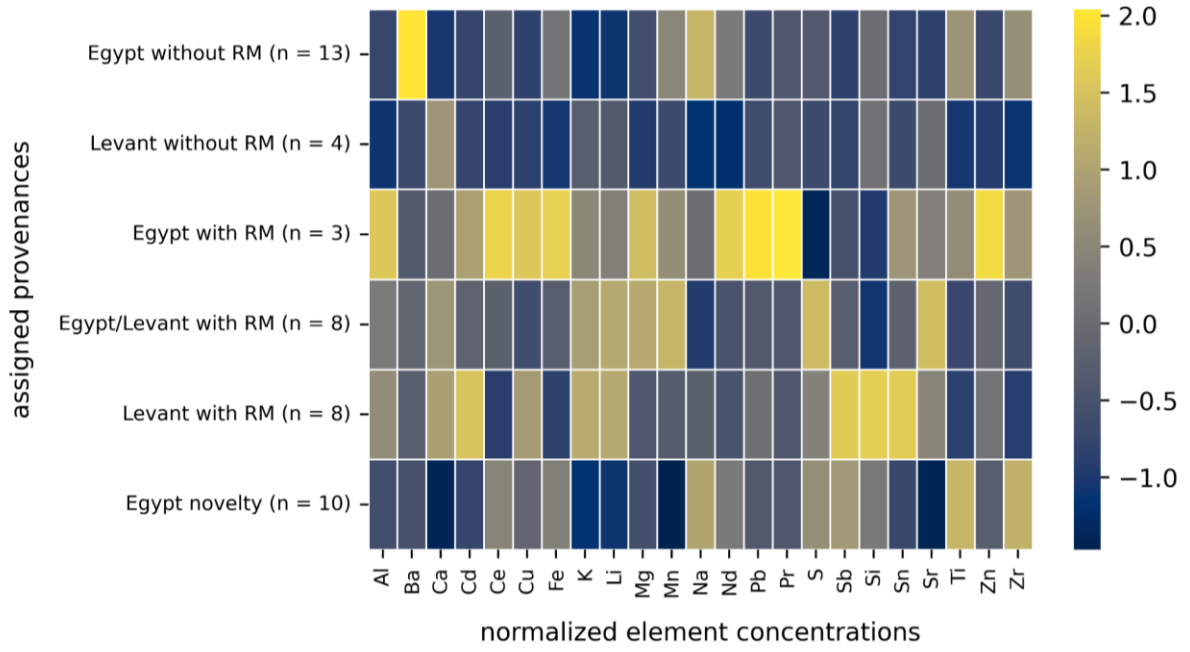

Figure 4.19: Heat map displaying the normalized means of the element compositions of the different assigned groups; n = number of samples assigned to the group

When examining the samples without RMs, significant discrepancies between the provenances Egypt and Levant can be observed in elements such as Ba and Na, but also Ti, Ca, Fe, and Zr. As already introduced in Figure 2.1 these elements represent the use of different raw materials for sand, limestone and natron.

Regarding the recycled glasses, the observable higher levels of K and Mg also indicate the remelting of the glass. These elements could have been introduced into the material by the fuel ash of the furnaces used. [11]

Furthermore, the novel Egyptian glasses demonstrate similarities to established Egyptian glass types, with similarly elevated Na, Ti and Zr levels, while the Ba concentration is lower.

Using an algorithm can present a drawback in terms of difficulty in tracing back the weight of the features used. To address this concern and to visually reinforce the observations made earlier, a PCA was conducted on the samples, utilizing all the element concentrations as features (see Figure 4.20, Figure 4.21). In these two figures the resulting principal component 1 (PC 1) and principal component 2 (PC 2) were plotted and the samples colored in two different ways to visualize similarities between the group members.

In Figure 4.20 the samples with RM, without RM and found novelties are colored differently. By examining the loadings, it becomes evident that the RMs, like for example Cu or Pb, for some samples distinctly differentiate the recycled samples from the others. Nevertheless, plotting PC 1 and PC 2 in this case does not differentiate between novel glasses and unrecycled glasses.

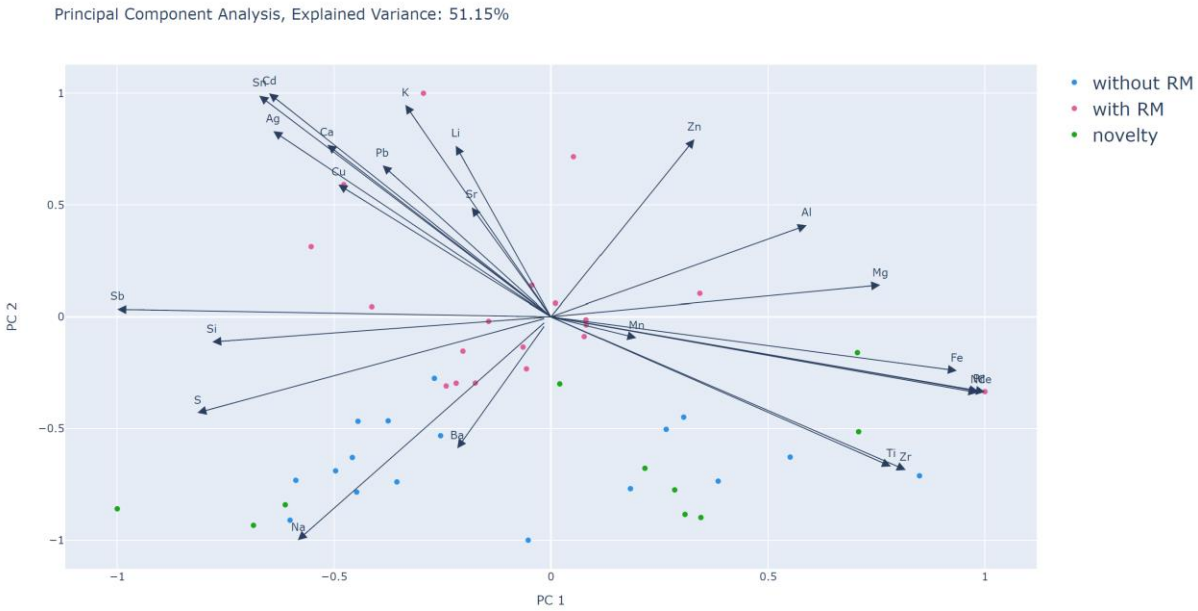

Figure 4.20: PCA of samples with all element concentrations measured, color coded by detected Recycling markers and Novelty detection

In Figure 4.21 the samples assigned to different provenances are colored differently. The loadings show that the elements indicating the provenance, which were already mentioned earlier in this chapter, like for example Ti, Zr or Na, separate the large and diffuse data clouds.

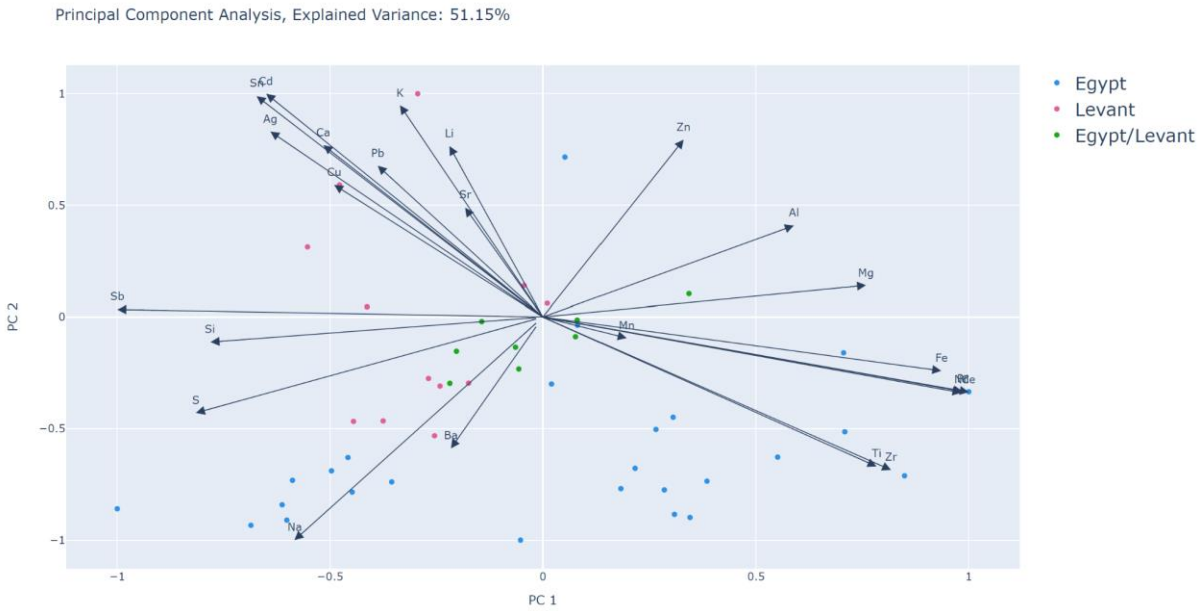

Figure 4.21: PCA of samples with all element concentrations measured, color coded by primary workshop location

Looking at this PCA in these two figures, it is essential to consider that with only two principal components plotted, only approximately 50% of the variance of the data can be explained. The large and diffuse data clouds cannot be visually separated, which again underlines the necessity for a classifying algorithm in this context.

5 Conclusion and Outlook

In conclusion this study on the elemental analysis of late-antique glass samples has provided valuable insights into the composition and origins of these ancient artifacts. By incorporating LIBS alongside the routine LA-ICP-MS setup, this research shed light on the advantages of Tandem-LIBS-LA-ICP-MS for the analysis of historical glass.

By the comparison of solid measurements to liquid measurements, it is proven that quantification with LIBS, together with the sum normalization method, in comparison to LA-ICP-MS could provide more precise results for the key components Ca and Al, while showing the same performance for Sr and Ba. However, K, Fe and Mn, crucial components for distinguishing late-antique glasses, were more accurately quantified using LA-ICP-MS. Nevertheless, it is important to consider that by substituting LA-ICP-MS measurements with LIBS for certain elements, we can free up additional acquisition time for analyzing other elements, which becomes relevant when using a quadrupole as a mass analyzer. This, in turn, can lead to improved precision in the results. Furthermore LIBS provides the advantage of conducting a non-targeted analysis of unknown samples, enabling the creation of a spectrum that serves as a unique fingerprint for the sample. This eliminates the need for preliminary survey scans and allows for the exploration of elements that may not have been previously considered, essentially treating the entire periodic table of elements as a canvas for investigation. This includes elements that are typically inaccessible to LA-ICP-MS, such as O, N and H.

Moreover, the study demonstrated the effectiveness of employing classification algorithms to classify late-antique glasses. This approach allowed for comparisons against a large reference dataset, even without prior archaeological knowledge of the samples. Through the use of OCSVM, the research identified 15 glasses as novel, differing in their base composition from the reference dataset, and revealed that 17 glasses were recycled. The development of two k-NN models, achieving impressive accuracies of 99% for distinguishing between Egypt and Levant provenances (k-NN P) and 91% for classifying into the established glass types (k-NN GT), was a significant achievement. For the novel and the recycled glasses, the classification result is seen as a proof of similarity between the samples and the reference glass type, which can help unravel the origin of these artifacts.

The reference database was constructed exclusively using base compositions gathered from literature sources. Sample base compositions were assessable through LIBS, allowing both Novelty detection and the training of the two k-NN models using LIBS data exclusively. LA-ICP-MS is solely required for trace element analysis in the glass. It is worth considering that while the current Tandem-LIBS-LA-ICP-MS setup is effective and necessary, using more

appropriate reference materials for quantification and dedicating additional time to select specific RMs could enable the use of an ICCD detector for more sensitive LIBS measurements, specifically tailored for certain trace elements. This could potentially eliminate the need for LA-ICP-MS. This approach would unlock the advantages of exclusive LIBS measurements, including handheld applications, which would be highly beneficial for archaeologists working in the field, enabling rapid glass analysis. To enhance the statistical evaluation, expanding the dataset with more reference glasses would be beneficial. With sufficient data, trace elements could also be incorporated into the dataset, thereby improving the modelling of the algorithms.

It is important to note that this work should not be considered in isolation. The author rightly acknowledges the essential role of archaeologists in providing the broader context for these findings. Archaeological expertise is crucial for validating the plausibility of the results and further enhancing our understanding of these ancient artifacts. In essence, this study serves as a bridge between the fields of chemistry and archaeology, demonstrating how advanced analytical techniques can unlock the secrets of ancient materials. Its results pave the way for collaborative efforts between chemists and archaeologists, fostering a deeper comprehension of historical civilizations and their technological achievements. This work stands as a testament to the interdisciplinary nature of research and the need for cross-disciplinary cooperation to unravel the mysteries of our past.

6 References

[1] P. Degryse, Ed., *Glass Making in the Greco-Roman World*. Leuven University Press, 2014.

[2] B. Wagner, A. Nowak, E. Bulska, J. Kunicki-Goldfinger, O. Schalm, and K. Janssens, "Complementary analysis of historical glass by scanning electron microscopy with energy dispersive X-ray spectroscopy and laser ablation inductively coupled plasma mass spectrometry," *Microchim. Acta*, vol. 162, no. 3–4, pp. 415–424, 2008, doi: 10.1007/s00604-007-0835-7.

[3] A. Bonneau *et al.*, "Archaeometrical Analysis of Glass Beads: Potential , Limitations , and Results," *BEADS J. Soc. Bead Res.*, vol. 26, pp. 35–46, 2014.

[4] D. Chew, K. Drost, J. H. Marsh, and J. A. Petrus, "LA-ICP-MS imaging in the geosciences and its applications to geochronology," *Chem. Geol.*, vol. 559, no. June 2020, p. 119917, 2021, doi: 10.1016/j.chemgeo.2020.119917.

[5] M. Binder, J. Eitler, J. Deutschmann, S. Ladstätter, F. Glaser, and D. Fiedler, "Prosthetics in antiquity-An early medieval wearer of a foot prosthesis (6th century AD) from Hemmaberg/Austria," *Int. J. Paleopathol.*, vol. 12, pp. 29–40, 2016, doi: 10.1016/j.ijpp.2015.11.003.

[6] P. Scherrer, *Die 50 bekanntesten archäologischen Stätten in Österreich*. Mainz: Nünnerich Asmus Verlag & Media, 2016.

[7] A. K. Varshneya and J. C. Mauro, *Fundamentals of inorganic glasses*, 3rd ed. Amsterdam, Netherlands: Elsevier, 2019.

[8] "ICG | International Comission on Glass." [Online]. Available: https://icglass.org/. [Accessed: 13-Jan-2023].

[9] I. C. Freestone, "Glass production in Late Antiquity and the Early Islamic period: A geochemical perspective," *Geol. Soc. Spec. Publ.*, vol. 257, pp. 201–216, 2006, doi: 10.1144/GSL.SP.2006.257.01.16.

[10] S. Paynter and C. Jackson, "Re-used Roman rubbish: a thousand years of recycling glass," *Post-Classical Archaeol.*, vol. 6, pp. 31–52, 2016.

[11] I. C. Freestone, "The Recycling and Reuse of Roman Glass: Analytical Approaches," *J. Glass Stud.*, pp. 29–40, 2015.

[12] D. Brems and P. Degryse, "Trace Element Analysis in Provenancing Roman Glass-Making," *Archaeometry*, vol. 56, pp. 116–136, 2014, doi: 10.1111/ARCM.12063.

[13] R. Bugoi, A. Panaite, and C. G. Alexandrescu, "Chemical analyses on Roman and Late Antique glass finds from the Lower Danube: the case of Tropaeum Traiani," *Archaeol. Anthropol. Sci.*, vol. 13, no. 9, 2021, doi: 10.1007/s12520-021-01310-7.

[14] D. A. Skoog, F. J. Holler, and S. R. Crouch, *Principles of instrumental analysis*, Seventh edition. Boston, MA: Cengage Learning, 2018.

[15] M. W. Sigrist, *Laser: Theorie, Typen und Anwendungen*, 8th ed. Berlin: Springer Spektrum, 2018.

[16] R. E. Russo, X. Mao, H. Liu, J. Gonzalez, and S. S. Mao, “Laser ablation in analytical chemistry—a review,” *Talanta*, vol. 57, no. 3, p. 425, 2002, doi: 10.1016/S0039-9140(02)00053-X.

[17] X. Mao and R. E. Russo, “Observation of plasma shielding by measuring transmitted and reflected laser pulse temporal profiles,” *Appl. Phys. A*, vol. 64, no. 1, pp. 1–6, 1996, doi: 10.1007/s003390050437.

[18] D. A. Cremers and L. J. Radziemski, *Handbook of Laser-Induced Breakdown Spectroscopy*, 2nd ed. Chichester: John Wiley and Sons, 2013.

[19] A. Limbeck *et al.*, “Methodology and applications of elemental mapping by laser induced breakdown spectroscopy,” *Anal. Chim. Acta*, vol. 1147, pp. 72–98, 2021, doi: https://doi.org/10.1016/j.aca.2020.12.054.

[20] L. Dussubieux, M. Golitko, and B. Gratuze, Eds., *Recent Advances in Laser Ablation ICP-MS for Archaeology*. Berlin Heidelberg: Springer Verlag, 2016.

[21] D. W. Koppenaal, G. C. Eiden, and C. J. Barinaga, “Collision and reaction cells in atomic mass spectrometry: development, status, and applications,” *J. Anal. At. Spectrom.*, vol. 19, no. 5, pp. 561–570, 2004, doi: 10.1039/B403510K.

[22] A. C. Müller and S. Guido, *Introduction to machine learning with Python: a guide for data scientists*, 1st ed. Sebastopol, CA: O’Reilly Media, 2017.

[23] L. Brunnbauer, Z. Gajarska, H. Lohninger, and A. Limbeck, “A critical review of recent trends in sample classification using Laser-Induced Breakdown Spectroscopy (LIBS),” *Trends Anal. Chem.*, vol. 159, 2023, doi: 10.1016/J.TRAC.2022.116859.

[24] A. Mammone, M. Turchi, and N. Cristianini, “Support vector machines,” *Wiley Interdiscip. Rev. Comput. Stat.*, vol. 1, no. 3, pp. 283–289, 2009, doi: 10.1002/wics.49.

[25] H. J. Shin, D.-H. Eom, and S.-S. Kim, “One-class support vector machines—an application in machine fault detection and classification,” *Comput. Ind. Eng.*, vol. 48, no. 2, pp. 395–408, 2005, doi: https://doi.org/10.1016/j.cie.2005.01.009.

[26] H. Abdi and L. J. Williams, “Principal component analysis,” *Wiley Interdiscip. Rev. Comput. Stat.*, vol. 2, no. 4, pp. 433–459, 2010, doi: 10.1002/wics.101.

[27] Y. Liu *et al.*, “In situ analysis of major and trace elements of anhydrous minerals by LA-ICP-MS without applying an internal standard,” *Chem. Geol.*, vol. 257, no. 1–2, pp. 34–43, 2008, doi: 10.1016/j.chemgeo.2008.08.004.

[28] T. R. Schöberl, “Determination of the mobile ion fraction in molding composite materials: influence of time and temperature,” Technische Universität Wien, 2023.

[29] R. Balvanović and Šmit, “Sixth-century AD glassware from Jelica, Serbia—an increasingly complex picture of late antiquity glass composition,” *Archaeol. Anthropol. Sci.*, vol. 12, no. 4, 2020, doi: 10.1007/s12520-020-01031-3.

[30] R. Balvanović, Šmit, M. M. Stojanović, D. Spasić-Đurić, P. Špehar, and O. Milović, “Late Roman glass from Viminacium and Egeta (Serbia): glass-trading patterns on Iron Gates Danubian Limes,” *Archaeol. Anthropol. Sci.*, vol. 14, no. 4, pp. 0–24, 2022, doi:

10.1007/s12520-022-01529-y.

[31] G. H. Barfod, I. C. Freestone, R. E. Jackson-Tal, A. Lichtenberger, and R. Raja, “Exotic glass types and the intensity of recycling in the northwest Quarter of Gerasa (Jerash, Jordan),” *J. Archaeol. Sci.*, vol. 140, p. 105546, 2022, doi: 10.1016/j.jas.2022.105546.

[32] C. Bertini, J. Henderson, and S. Chenery, “Seventh to eleventh century CE glass from Northern Italy: between continuity and innovation,” *Archaeol. Anthropol. Sci.*, vol. 12, no. 6, 2020, doi: 10.1007/s12520-020-01048-8.

[33] A. I. Bidegaray *et al.*, “On the making, mixing and trading of glass from the Roman military fort at Oudenburg (Belgium),” *Archaeol. Anthropol. Sci.*, vol. 11, no. 6, pp. 2385–2405, 2019, doi: 10.1007/s12520-018-0680-0.

[34] C. Boschetti, J. Kindberg Jacobsen, C. Parisi Presicce, R. Raja, N. Schibille, and M. Vitti, “Glass in Rome during the transition from late antiquity to the early Middle Ages: materials from the Forum of Caesar,” *Herit. Sci.*, vol. 10, no. 1, pp. 1–14, 2022, doi: 10.1186/s40494-022-00729-y.

[35] R. H. Brill, “Scientific investigations of the Jalame glass and related finds,” in *Excavations at Jalame: site of a glass factory in late Roman Palestine*, G. D. Weinberg, Ed. Columbia: University of Missouri Press, 1988, pp. 257–295.

[36] R. Bugoi *et al.*, “Shedding Light on Roman Glass Consumption on the Western Coast of the Black Sea,” *Materials (Basel).*, vol. 15, no. 2, pp. 1–15, 2022, doi: 10.3390/ma15020403.

[37] A. Ceglia, P. Cosyns, K. Nys, H. Terryn, H. Thienpont, and W. Meulebroeck, “Late antique glass distribution and consumption in Cyprus: A chemical study,” *J. Archaeol. Sci.*, vol. 61, pp. 213–222, 2015, doi: 10.1016/j.jas.2015.06.009.

[38] A. Cholakova, T. Rehren, and I. C. Freestone, “Compositional identification of 6th c. AD glass from the Lower Danube,” *J. Archaeol. Sci. Reports*, vol. 7, pp. 625–632, 2016, doi: 10.1016/j.jasrep.2015.08.009.

[39] S. Conte, T. Chinni, R. Arletti, and M. Vandini, “Butrint (Albania) between eastern and western Mediterranean glass production: EMPA and LA-ICP-MS of late antique and early medieval finds,” *J. Archaeol. Sci.*, vol. 49, no. 1, pp. 6–20, 2014, doi: 10.1016/j.jas.2014.04.014.

[40] J. De Juan Ares and N. Schibille, “Glass import and production in Hispania during the early medieval period: The glass from Ciudad de Vascos (Toledo),” *PLoS One*, vol. 12, no. 7, pp. 1–19, 2017, doi: 10.1371/journal.pone.0182129.

[41] J. De Juan Ares, A. Vigil-Escalera Guirado, Y. Cáceres Gutiérrez, and N. Schibille, “Changes in the supply of eastern Mediterranean glasses to Visigothic Spain,” *J. Archaeol. Sci.*, vol. 107, pp. 23–31, 2019, doi: 10.1016/j.jas.2019.04.006.

[42] J. de Juan Ares, N. Schibille, J. M. Vidal, and M. D. Sánchez de Prado, “The Supply of Glass at Portus Ilicitanus (Alicante, Spain): A Meta-Analysis of HIMT Glasses,” *Archaeometry*, vol. 61, no. 3, pp. 647–662, 2019, doi: 10.1111/arcm.12446.

[43] H. E. Foster and C. M. Jackson, “The composition of ‘naturally coloured’ late Roman

vessel glass from Britain and the implications for models of glass production and supply," *J. Archaeol. Sci.*, vol. 36, no. 2, pp. 189–204, 2009, doi: 10.1016/j.jas.2008.08.008.

[44] D. Foy, M. Picon, M. Vichy, and V. Thirion-Merle, "Caractérisation des verres de la fin de l'Antiquité en Méditerranée occidentale : l'émergence de nouveaux courants commerciaux," *Echanges Commer. du verre dans le monde Antiq.*, pp. 41–85, 2003.

[45] E. Gliozzo, A. S. Barbone, and F. D'Acapito, "Waste glass, vessels and window-panes from thamusida (Morocco): Grouping natron-based blue-green and colourless roman glasses," *Archaeometry*, vol. 55, no. 4, pp. 609–639, 2013, doi: 10.1111/j.1475-4754.2012.00696.x.

[46] S. Maltoni, A. Silvestri, A. Marcante, and G. Molin, "The transition from Roman to Late Antique glass: new insights from the Domus of Tito Macro in Aquileia (Italy)," *J. Archaeol. Sci.*, vol. 73, pp. 1–16, 2016, doi: 10.1016/j.jas.2016.07.002.

[47] M. Phelps, I. C. Freestone, Y. Gorin-Rosen, and B. Gratuze, "Natron glass production and supply in the late antique and early medieval Near East: The effect of the Byzantine-Islamic transition," *J. Archaeol. Sci.*, vol. 75, pp. 57–71, 2016, doi: 10.1016/j.jas.2016.08.006.

[48] N. Schibille *et al.*, "Comprehensive Chemical Characterisation of Byzantine Glass Weights," *PLoS One*, vol. 11, no. 12, pp. 1–26, 2016, doi: 10.1371/journal.pone.0168289.

[49] N. Schibille, B. Gratuze, E. Ollivier, and É. Blondeau, "Chronology of early Islamic glass compositions from Egypt," *J. Archaeol. Sci.*, vol. 104, pp. 10–18, 2019, doi: 10.1016/j.jas.2019.02.001.

[50] A. Silvestri, "The coloured glass of Iulia Felix," *J. Archaeol. Sci.*, vol. 35, no. 6, pp. 1489–1501, 2008, doi: 10.1016/j.jas.2007.10.014.

[51] A. Silvestri, G. Molin, and G. Salviulo, "The colourless glass of Iulia Felix," *J. Archaeol. Sci.*, vol. 35, no. 2, pp. 331–341, 2008, doi: 10.1016/j.jas.2007.03.010.

[52] H. M. Spencer, K. R. Murdoch, J. Buckman, A. M. Forster, and C. J. Kennedy, "Compositional Analysis by p-XRF and SEM–EDX of Medieval Window Glass from Elgin Cathedral, Northern Scotland," *Archaeometry*, vol. 60, no. 5, pp. 1018–1035, 2018, doi: 10.1111/arcm.12357.

[53] A. Limbeck, P. Galler, M. Bonta, G. Bauer, W. Nischkauer, and F. Vanhaecke, "Recent advances in quantitative LA-ICP-MS analysis: challenges and solutions in the life sciences and environmental chemistry," *Anal. Bioanal. Chem.*, vol. 407, no. 22, pp. 6593–6617, 2015, doi: 10.1007/s00216-015-8858-0.

[54] L. Casanova *et al.*, "Evaluation of limits of detection in laser-induced breakdown spectroscopy: Demonstration for food," *Spectrochim. Acta Part B At. Spectrosc.*, vol. 207, p. 106760, 2023, doi: https://doi.org/10.1016/j.sab.2023.106760.

[55] T. W. May and R. H. Wiedmeyer, "A Table of Polyatomic Interferences in ICP-MS Isotope Abundance Interference," *At. Spectrosc.*, vol. 19, no. 5, pp. 150–155, 1998.

[56] N. Schibille, A. Sterrett-Krause, and I. C. Freestone, “Glass groups, glass supply and recycling in late Roman Carthage,” *Archaeol. Anthropol. Sci.*, vol. 9, no. 6, pp. 1223–1241, 2017, doi: 10.1007/s12520-016-0316-1.

[57] A. Ceglia, P. Cosyns, N. Schibille, and W. Meulebroeck, “Unravelling provenance and recycling of late antique glass from Cyprus with trace elements,” *Archaeol. Anthropol. Sci.*, vol. 11, no. 1, pp. 279–291, 2019, doi: 10.1007/s12520-017-0542-1.

[58] B. Gratuze, I. Pactat, and N. Schibille, “Changes in the Signature of Cobalt Colorants in Late Antique and Early Islamic Glass Production,” *Minerals*, vol. 8, no. 6, 2018, doi: 10.3390/min8060225.

[59] P. Degryse *et al.*, “Evidence for glass ‘recycling’ using Pb and Sr isotopic ratios and Sr-mixing lines: the case of early Byzantine Sagalassos,” *J. Archaeol. Sci.*, vol. 33, no. 4, pp. 494–501, Apr. 2006, doi: 10.1016/J.JAS.2005.09.003.

7 List of tables

8 List of figures

9 Appendix

Figure 9.1: Images of original artifacts before sampling

Table 9.1: Detailed information on sampled artifacts

work ID	description of artifact	transparency	color
HEMMA-GL-1	unformed primary glass	yes	brownish green
HEMMA-GL-2	unformed primary glass	yes	brownish green
HEMMA-GL-3	field fire	yes	green
HEMMA-GL-4	unformed primary glass	yes	brownish green
HEMMA-GL-5	unformed primary glass	yes	blue-green
HEMMA-GL-8	fragment of rim	yes	blue-green
HEMMA-GL-9	fragment of rim	yes	light blue-green / colorless
HEMMA-GL-10	fragment of wall	yes	blue
HEMMA-GL-11	fragment of rim	yes	blue
HEMMA-GL-13	fragment of rim	yes	light blue-green / colorless
HEMMA-GL-14	fragment of wall	yes	blue
HEMMA-GL-15	fragment of rim	yes	light blue-green / colorless
HEMMA-GL-16	fragment of rim	yes	green
HEMMA-GL-17	fragment of rim	yes	light blue-green
HEMMA-GL-18	fragment of rim	yes	colorless
HEMMA-GL-19	small handle	yes	colorless
HEMMA-GL-21	fragment of rim	yes	colorless
HEMMA-GL-22	fragment of rim	yes	colorless
HEMMA-GL-23	primary glass?	yes	colorless
HEMMA-GL-25	field fire	yes	colorless
HEMMA-GL-26	fragment of rim	yes	colorless to light brown
HEMMA-GL-27	fragment of rim	yes	colorless to light brown
HEMMA-GL-28	fragment of lid	yes	colorless to light brown
HEMMA-GL-29	fragment of rim of a bottle	yes	colorless to light blue-green
HEMMA-GL-30	fragment of lid	yes	bottlegreen
HEMMA-GL-31	fragment of rim	yes	bottlegreen
HEMMA-GL-32	fragment of rim	yes	colorless to light blue-green
HEMMA-GL-33	fragment of rim	yes	bottlegreen
HEMMA-GL-34	field fire	yes	colorless to light brown
HEMMA-GL-37	fragment of rim, in thickness alternating, wavelike ornaments of the glass	milky	green
HEMMA-GL-38	field fire	yes	light brown
HEMMA-GL-39	fragment of a thick rim	milky	green
HEMMA-GL-40	field fire	yes	green
HEMMA-GL-41	primary glass or field fire?	milky	green
HEMMA-GL-42	fragment of rim of a bottle	yes	bottlegreen
HEMMA-GL-43	field fire	yes	light blue-green
HEMMA-GL-44	fragment of rim	yes	light blue-green
HEMMA-GL-45	fragment of plate?	milky	green
HEMMA-GL-46	fragment of bottle bottom	yes	bottlegreen
HEMMA-GL-47	fragment of rim, horizontally applied bottlegreen cordon-like transparent ornaments	yes	colorless/bottlegreen
HEMMA-GL-48	fragment of rim	yes	colorless to light blue-green
HEMMA-GL-49	fragment of rim	yes	colorless to light blue-green
HEMMA-GL-50	fragment of lid	yes	light blue-green
HEMMA-GL-51	fragment of rim	yes	bottlegreen
HEMMA-GL-53	fragment of rim	yes	bottlegreen

HEMMA-GL-54	fragment of rim	yes	colorless to light bottle green

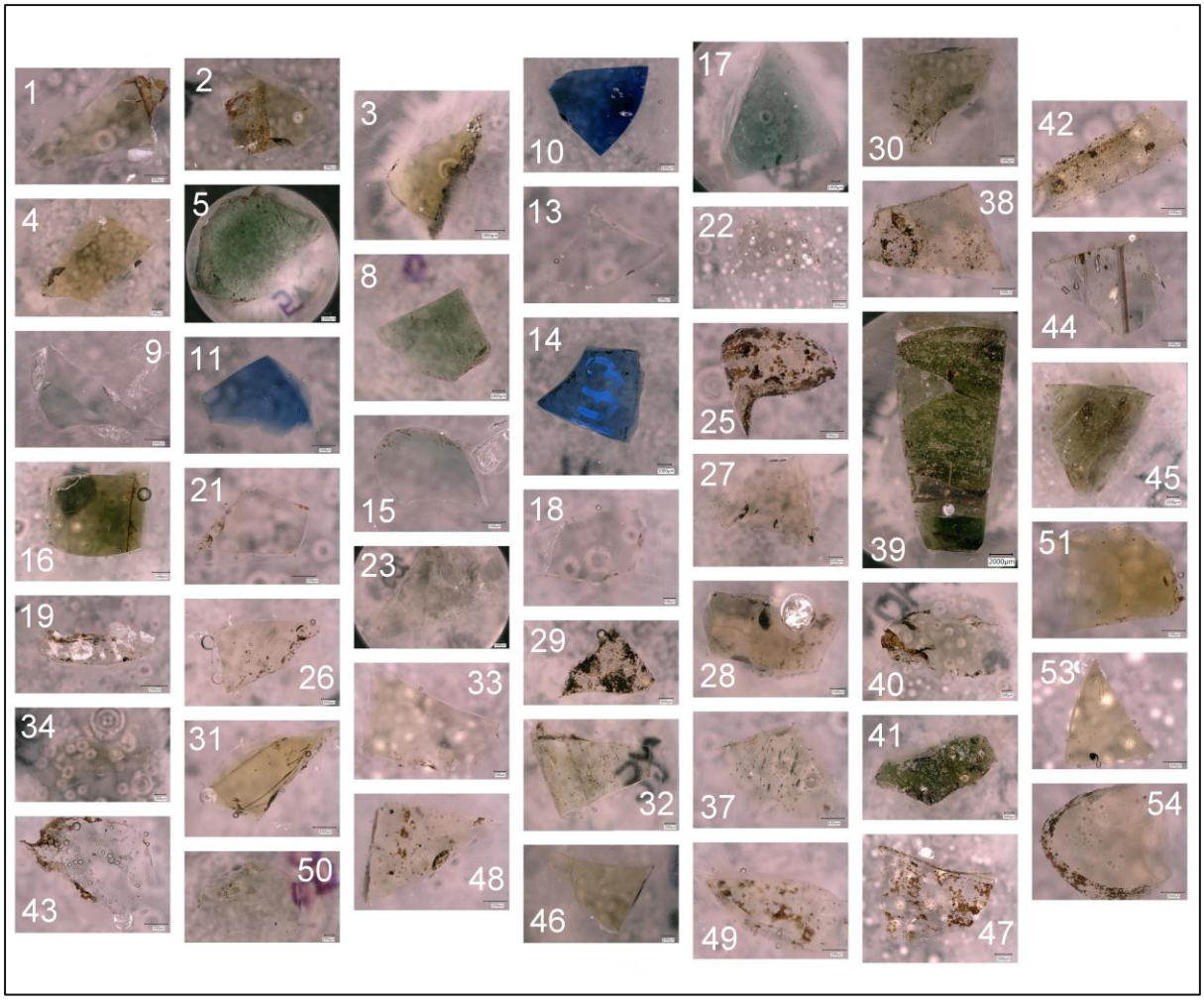

Figure 9.2: Microscopic images of all analyzed samples

Table 9.2: List of used standard solutions for quantification of the liquid measurement

Element	Concentration [mg/L]	Supplier
Al	100	Merck Supelco (multi-element standard solution VIII)
Ba	100	Merck Supelco (multi-element standard solution VIII)
Ca	97	Merck Supelco (multi-element standard solution VIII)
Ce	1005	Alfa Aesar
Co	97	Merck Supelco (multi-element standard solution VIII)
Cu	99	Merck Supelco (multi-element standard solution VIII)
Eu	993	Alfa Aesar
Fe	100	Merck Supelco (multi-element standard solution VIII)
Gd	986	Merck
K	100	Merck Supelco (multi-element standard solution VIII)
La	1004	Thermo Scientific

Li	100	Merck Supelco (multi-element standard solution VIII)
Mg	100	Merck Supelco (multi-element standard solution VIII)
Mn	100	Merck Supelco (multi-element standard solution VIII)
Na	100	Merck Supelco (multi-element standard solution VIII)
Nd	1000	VWR
Ni	101	Merck Supelco (multi-element standard solution VIII)
P	993	Thermo Scientific
Pb	99	Merck Supelco (multi-element standard solution VIII)
Pr	989	VWR
S	1002	Alfa Aesar
Sb	967	Merck
Sc	972	Merck
Sn	970	Merck Supelco
Sr	100	Merck Supelco (multi-element standard solution VIII)
Ti	999	Merck
Yb	980	Alfa Aesar
Zn	103	Merck Supelco (multi-element standard solution VIII)
Zr	963	Merck
Y	988	Merck Supelco

Table 9.3: Sample weights for digestion

	sample number	weighted sample [g]			sample number	weighted sample [g]
batch 1	aG15	0.0356		batch 4	aG3	0.0304
	aG16	0.0352			aG4	0.0305
	aG26	0.0295			aG25	0.031
	aG33	0.0278			aG28	0.0335
	aG41	0.0321			aG29	0.0355
	aG46	0.0342			aG34	0.0317
	aG51	0.0337			aG40	0.0303
batch 2	aG2	0.028		batch 5	aG9	0.0307
	aG5	0.0307			aG17	0.0275
	aG13	0.0359			aG23	0.0299
	aG30	0.0352			aG27	0.0359
	aG37	0.033			aG39	0.0351
	aG38	0.0347			aG43	0.0306
	aG42	0.0371			aG48	0.0308
batch 3	aG1	0.0326				
	aG11	0.0328				
	aG18	0.0313				
	aG21	0.0349				
	aG45	0.0312				
	aG47	0.0341				
	aG50	0.0318				

Table 9.4: Results for liquid measurement with ICP-OES

	Element concentrations for measurements with ICP-OES [µg/g]																								
sample #	Al	Ba	Ca	Ce	Co	Cu	Eu	Fe	K	La	Li	Mg	Mn	Na	Ni	P	S	Sb	Sc	Sr	Ti	Y	Yb	Zn	Zr
1	10499	366	45498	26	10	135	< LOD	11469	7962	8	7	4600	12259	116516	8	868	1662	< LOD	0	668	1182	9	23	31	114
2	13163	412	50994	1	9	165	< LOD	13177	8556	6	7	6744	14817	118413	8	1032	2019	< LOD	1	729	1235	10	28	41	108
3	15746	531	34361	13	10	55	< LOD	15492	4207	11	4	7864	22038	139941	0	232	1499	< LOD	< LOD	438	4194	13	47	33	360
4	14571	404	50295	< LOD	< LOD	155	< LOD	13089	8345	12	10	7938	14679	115805	< LOD	1017	1753	< LOD	1	719	1197	9	26	38	107
5	11267	315	50334	< LOD	22	591	< LOD	6463	7088	8	6	4802	6444	123548	< LOD	665	1663	1045	< LOD	472	928	7	10	64	83
9	12212	153	35538	25	< LOD	7	< LOD	10717	3105	3	4	5286	474	138784	< LOD	200	1498	< LOD	< LOD	405	3525	13	< LOD	30	324
11	11664	150	39767	< LOD	1315	1818	< LOD	13225	3016	4	4	5190	961	153090	27	219	2292	< LOD	< LOD	450	1798	9	2	56	160
13	12053	218	52606	< LOD	10	1	< LOD	2832	5665	4	6	3156	2438	109600	< LOD	834	1096	61	< LOD	464	418	7	5	13	39
15	14533	156	36767	21	< LOD	4	< LOD	11191	2946	3	3	7057	423	142677	< LOD	216	1596	< LOD	< LOD	411	3583	11	< LOD	30	318
16	9649	256	32196	18	8	75	< LOD	12760	4619	6	3	4808	8955	111259	14	534	1473	< LOD	< LOD	414	1702	8	8	29	138
17	12074	223	45765	7	7	595	< LOD	4898	6105	4	3	4129	2978	122308	< LOD	732	1274	394	< LOD	412	1027	6	10	31	91
18	8221	220	45119	< LOD	4	15	< LOD	3101	2751	6	1	3191	5633	145279	< LOD	43	2099	49	0	495	471	5	12	15	43
21	7477	255	51331	< LOD	< LOD	20	< LOD	5244	4110	11	7	3055	9327	128605	< LOD	238	1994	103	0	651	689	7	20	85	65
23	8218	137	34759	23	< LOD	9	< LOD	1981	2970	< LOD	2	2288	86	143738	< LOD	75	1588	3732	< LOD	363	326	4	< LOD	20	32
25	11467	272	52129	19	5	30	< LOD	5312	5844	6	5	5994	11367	148809	< LOD	450	2468	201	< LOD	733	778	8	23	28	73
26	3689	345	24941	< LOD	2	57	< LOD	5114	6665	3	7	2479	13085	139199	< LOD	597	2085	141	< LOD	567	948	1	33	36	42
27	11883	326	51983	9	< LOD	69	< LOD	6583	5906	5	8	6693	13251	133706	2	590	2098	57	0	707	858	8	28	23	76
28	12206	346	57081	41	< LOD	99	< LOD	6773	6611	9	8	6789	14815	129918	6	543	2408	4	0	873	915	7	31	30	84
29	10017	310	44424	< LOD	4	33	< LOD	4924	4431	6	6	4028	8937	150076	21	130	2194	93	0	581	667	7	17	14	66
30	4823	287	28848	25	10	66	< LOD	5954	8061	< LOD	7	3100	14268	131195	11	860	1919	23	< LOD	616	939	2	33	34	55
33	11082	280	35486	< LOD	< LOD	46	< LOD	15955	3520	16	4	6544	10552	138310	3	395	1467	< LOD	1	455	1485	9	21	27	112
34	12418	427	56483	34	2	80	< LOD	7035	6599	7	11	6932	14014	134705	6	614	2327	98	1	835	950	8	28	28	82
37	14384	1043	34507	2	3	45	< LOD	11085	4087	2	5	5954	15803	135016	5	151	1750	34	0	430	2799	10	28	39	231
38	12759	423	52398	1	< LOD	66	< LOD	7395	8230	8	14	7209	14169	139830	< LOD	538	2330	252	1	780	946	8	33	34	80
39	10732	1496	40091	16	11	71	< LOD	9396	4830	6	6	3691	15372	134405	3	315	1523	69	0	495	2057	10	34	26	167
40	13752	383	57486	< LOD	< LOD	68	< LOD	8258	9027	9	10	7417	12180	123698	22	585	2187	255	0	824	1035	9	21	28	91
41	14285	443	41077	4	< LOD	52	< LOD	18219	6895	9	7	6860	12875	126758	3	489	1368	< LOD	0	491	2696	12	25	52	212
42	14893	331	39939	5	< LOD	86	< LOD	24491	3757	9	5	7353	15639	125767	33	646	1501	< LOD	1	493	2724	14	28	45	215
43	8484	210	41560	31	< LOD	4	< LOD	3707	3685	1	5	3199	4815	145815	< LOD	< LOD	1279	< LOD	< LOD	477	620	6	11	21	65
45	12504	4513	31009	< LOD	< LOD	28	< LOD	9965	3096	3	6	5558	16421	121557	1	223	1242	< LOD	0	431	2269	10	28	23	183
46	8886	410	55549	14	4	51	< LOD	8226	5771	9	5	5453	14807	136204	26	495	2127	265	0	887	975	8	30	34	85
47	9692	354	38712	8	< LOD	14	< LOD	3848	3634	8	5	3879	7450	140813	10	54	2231	124	< LOD	410	475	6	13	20	52
48	12135	335	55141	17	< LOD	83	< LOD	6740	6505	10	9	6598	14085	125384	< LOD	600	2245	27	1	843	902	8	27	28	84
50	9419	238	45048	19	11	22	< LOD	4900	2758	7	4	4598	7552	146776	11	127	1721	< LOD	0	509	594	6	13	19	54
51	12064	316	44172	21	< LOD	77	< LOD	24741	2646	9	4	5737	13753	151758	3	477	2081	< LOD	< LOD	503	3206	15	34	30	288

Table 9.5: Results for liquid measurement with ICP-MS

	Element concentrations for measurements with ICP-MS [µg/g]									
sample #	Ag	Au	Bi	Cd	Ce	Gd	Nd	Pb	Pr	Sn
1	0.09	< LOD	< LOD	0.90	14.81	4.85	10.36	281.25	2.29	11.45
2	0.14	< LOD	0.05	1.09	16.45	5.30	11.50	307.96	2.51	12.88
3	0.16	0.01	< LOD	0.81	24.58	6.52	15.71	9.22	3.17	2.07
4	0.11	< LOD	< LOD	1.00	16.67	5.50	11.70	305.45	2.63	13.07
5	1.02	< LOD	0.15	6.38	13.15	3.86	9.51	1315.57	1.82	107.39
9	0.14	< LOD	< LOD	0.68	33.30	4.58	16.93	7.70	3.21	2.00
11	0.20	< LOD	< LOD	1.25	15.69	3.21	10.07	1565.41	2.08	16.64
13	0.01	< LOD	< LOD	0.07	12.19	3.14	8.07	8.71	1.65	0.47
15	0.16	0.00	0.01	0.68	20.19	3.81	12.96	7.02	2.63	1.06
16	0.13	< LOD	< LOD	0.52	9.79	3.19	7.57	120.02	1.71	5.22
17	0.36	< LOD	0.01	5.00	14.04	3.22	8.93	178.85	1.85	85.23
18	0.03	< LOD	< LOD	0.25	10.33	2.83	7.00	17.33	1.44	2.76
21	0.03	< LOD	0.04	0.91	12.86	3.44	10.05	23.66	2.73	3.47
23	0.22	< LOD	0.46	0.46	9.31	2.29	5.92	29.49	1.19	0.44
25	0.12	< LOD	< LOD	0.53	13.97	3.77	9.16	87.53	1.89	5.91
26	0.17	< LOD	0.06	1.02	3.46	2.39	2.27	103.33	0.48	15.39
27	0.11	< LOD	0.02	0.83	14.37	4.15	9.45	116.47	1.97	11.27
28	0.10	< LOD	< LOD	1.22	14.99	4.26	9.80	209.72	2.00	17.83
29	0.05	< LOD	< LOD	0.23	12.02	3.64	8.03	36.33	1.69	2.68
30	1.36	< LOD	< LOD	0.63	4.86	2.25	2.97	135.53	0.64	8.62
33	0.06	0.09	0.08	0.45	14.70	4.58	11.71	22.05	2.70	1.63
34	0.15	< LOD	< LOD	1.08	15.65	4.93	10.58	133.45	2.19	15.73
37	0.11	< LOD	< LOD	0.57	18.73	8.39	12.20	15.32	2.50	1.72
38	0.12	< LOD	< LOD	1.16	15.54	4.84	10.37	116.58	2.23	17.23
39	0.16	< LOD	< LOD	0.55	16.48	10.41	10.90	48.20	2.32	3.82
40	0.10	< LOD	0.02	0.68	16.79	4.68	11.10	108.99	2.31	8.91
41	0.19	< LOD	0.00	0.80	18.48	6.14	13.82	71.96	3.15	5.25
42	0.18	< LOD	0.02	0.56	19.49	6.41	16.23	37.86	3.87	2.32
43	0.02	< LOD	< LOD	0.14	10.75	2.71	7.08	7.77	1.45	0.93
45	0.08	< LOD	0.33	0.81	15.06	24.78	9.69	10.85	1.93	2.19
46	0.09	< LOD	0.03	0.60	14.80	4.61	9.97	85.43	2.18	6.88
47	0.01	< LOD	< LOD	0.14	11.26	3.65	7.51	8.50	1.55	1.09
48	0.11	< LOD	< LOD	1.13	14.70	4.06	9.79	204.17	2.02	16.27
50	0.01	< LOD	0.05	0.19	10.94	3.07	7.32	9.27	1.53	1.18
51	0.14	< LOD	0.10	0.79	20.11	6.27	16.09	16.81	3.77	1.38

Table 9.6: Results for solid measurement with LIBS

sample #	Element concentration [µg/g]										
	Al	Ba	Ca	Fe	K	Mg	Mn	Na	Si	Sr	Ti
1	12497	411	63569	12812	3126	3242	8114	111533	332246	726	843
2	11497	405	62128	13589	2993	3352	8701	106575	330551	688	832
3	12881	603	44723	15230	2279	3305	12456	131222	325021	554	3280

4	12615	445	65061	13549	3070	3298	8944	107736	323693	773	829
5	11309	353	65045	7325	2917	2729	5352	116911	336226	498	734
8	12270	266	52371	14421	1839	2995	4780	130040	327017	472	2824
9	11097	161	46037	11969	1749	2936	771	131859	330574	378	3031
10	12240	247	59304	17141	2587	2823	4088	133820	317643	576	1324
11	12614	188	45437	11225	1948	2765	700	137128	319369	423	2903
13	11791	239	68750	3177	2384	1848	1445	103803	329861	478	269
14	12181	319	66438	6085	3101	1990	5114	117013	331902	535	189
15	12759	192	45543	11212	1950	2761	705	137155	318586	430	2892
16	10848	340	55008	18608	2203	2928	7725	122336	322310	540	1759
17	11530	277	58834	3873	2922	2012	3131	118860	331736	446	305
18	9341	233	56437	2964	1693	1822	3886	143622	320926	503	241
19	7399	263	41637	3568	1757	1892	5401	130758	327319	395	297
21	10023	268	62708	5646	2140	2473	6525	122491	326656	635	380
22	8618	283	51743	4997	2135	2305	6548	132752	334363	492	417
23	7367	129	42193	2077	1708	1473	35	134377	330330	296	198
25	11333	319	65984	5411	2483	2885	5276	130867	323843	738	557
26	9325	336	56830	7375	2587	3124	7898	119341	328122	603	576
27	10365	312	58958	6837	2651	2906	8123	115609	318192	653	500
28	10031	293	66361	7321	2543	3065	7659	116981	330499	714	565
29	9576	316	50660	4553	2298	2090	6071	132210	321140	547	368
30	9778	293	58058	7620	2902	3165	8042	117164	329302	647	538
31	11015	347	56270	19906	2012	3111	10262	121306	319868	558	2420
32	8976	229	59795	5642	2088	2472	5486	117332	317715	569	509
33	9620	255	40524	17032	1831	3152	7205	117519	322905	392	1148
34	10945	392	62033	7439	2851	2985	8376	114913	321823	758	573
37	9969	629	39863	12397	1887	2868	9027	118046	337403	403	2664
38	10701	378	58388	7671	3276	3022	8426	118377	320898	701	540
39	9182	3790	38235	11212	1674	2629	8012	133867	326900	392	1968
40	12708	419	72104	8355	3457	3166	5458	115142	319813	805	791
41	14461	533	55659	18380	3395	3152	5722	119135	323900	549	2562
42	10982	309	49385	25623	1914	3158	9200	114975	330944	436	2421
43	7423	174	45705	3611	1837	1906	3355	131501	328787	369	398
44	10396	335	55536	5887	2938	2317	5082	120168	332993	447	603
45	11579	4055	37724	9675	2126	2563	9410	121346	332523	527	1911
46	12714	448	67866	8754	2703	3324	6638	121320	317760	926	642
47	10484	397	48280	4160	2096	1830	4006	130020	334103	461	281
48	13539	395	67402	6630	3593	2927	9306	127632	337972	960	464
49	9588	251	46588	4344	2034	2626	6498	130396	321483	454	350
50	9561	232	51332	4631	1861	2356	5269	138152	322800	472	280
51	12588	369	56845	24217	1558	3097	5663	135892	316325	475	3108
53	13364	328	48890	22213	2598	3353	8560	126289	320157	585	2076
54	10196	352	55359	6326	2987	2885	7672	124267	314749	644	475

Table 9.7: Results for solid measurement with LA-ICP-MS

sample #	Element concentration [µg/g]												
	Ag	Cd	Ce	Cu	Li	Nd	Pb	Pr	S	Sb	Sn	Zn	Zr
1	0.07	1.18	10.14	122.32	7.46	7.40	238.40	2.00	1073	19.51	10.11	37.84	57.18
2	0.07	1.14	9.93	129.96	7.52	7.33	227.10	1.98	1001	18.92	9.85	39.39	55.20
3	0.04	0.19	12.70	43.34	4.50	8.76	6.37	2.37	950	0.68	0.87	37.99	181.40
4	0.09	1.65	13.28	176.70	10.40	9.84	298.97	2.65	1261	21.46	13.29	36.88	72.99
5	1.12	11.40	9.59	624.65	8.53	6.80	1226.26	1.84	909	1151.17	103.27	64.77	54.98
8	0.05	0.27	13.13	21.05	4.14	9.37	10.64	2.53	955	0.68	1.52	25.15	171.10
9	0.04	0.18	14.35	5.78	4.55	9.82	7.33	2.68	1364	0.40	1.35	20.51	204.51
10	0.42	6.19	9.80	1665.75	6.42	6.88	3153.00	1.87	1612	209.26	67.91	90.43	85.97
11	0.12	1.37	10.05	1789.62	4.77	6.96	1311.77	1.89	2059	1.01	14.29	48.74	102.41
13	0.01	0.09	8.66	5.79	3.49	6.10	6.43	1.62	712	16.19	0.62	12.91	24.48
14	0.13	2.76	7.94	1276.14	3.58	5.69	116.43	1.51	779	195.52	30.31	38.50	24.11
15	0.04	0.14	13.25	4.27	4.06	9.12	6.32	2.48	1232	0.31	1.07	17.71	189.21
16	0.16	0.75	12.23	86.69	4.93	9.64	166.61	2.58	1262	6.52	7.62	39.68	100.20
17	0.41	8.82	8.29	734.15	4.94	5.78	189.47	1.55	946	672.12	95.00	29.29	32.39
18	0.03	0.28	7.25	17.30	3.35	5.21	15.38	1.39	1681	0.42	2.59	15.68	29.22
19	0.02	0.14	6.78	29.07	4.24	4.88	11.48	1.31	2124	0.94	1.14	12.25	30.19
21	0.02	0.32	7.86	17.34	5.59	5.55	17.29	1.50	1387	0.33	2.86	27.12	37.64
22	0.03	0.27	7.99	28.73	5.37	5.69	29.11	1.54	1941	65.06	2.52	19.38	40.57
23	0.20	0.08	6.18	11.11	2.77	4.37	26.89	1.18	1560	3916.79	0.30	18.70	20.95
25	0.14	0.76	9.43	66.06	6.67	6.58	76.60	1.80	2115	233.93	5.32	27.28	50.03
26	0.07	1.42	9.95	62.15	7.64	7.09	90.82	1.92	1915	189.71	14.45	29.96	52.34
27	0.08	0.89	8.68	63.19	7.28	6.08	94.04	1.64	1434	114.17	8.98	21.89	47.46
28	0.08	1.39	9.26	80.39	8.44	6.50	163.81	1.77	1712	137.27	14.07	29.14	51.42
29	0.05	0.24	8.03	28.08	6.75	5.69	22.42	1.53	1992	26.95	1.98	20.27	39.61
30	0.05	0.73	7.72	52.01	6.20	5.42	87.40	1.48	1483	73.34	7.12	31.71	45.62
31	0.12	0.75	10.26	56.77	4.23	7.82	72.11	2.11	1176	3.07	7.39	34.96	104.60
32	0.04	0.37	10.20	25.50	7.36	7.15	30.27	1.94	1729	1.71	3.61	16.98	55.48
33	0.02	0.22	11.96	45.32	5.35	9.50	19.42	2.55	1211	0.36	1.83	37.93	73.33
34	0.13	1.37	10.50	80.09	7.51	7.52	115.55	2.02	1694	111.23	13.72	30.56	53.43
37	0.04	0.17	13.14	45.29	4.92	9.16	9.07	2.47	1383	0.65	1.12	30.51	158.22
38	0.07	1.35	8.96	59.24	12.30	6.38	86.46	1.72	1663	194.98	13.45	33.44	46.61
39	0.05	0.12	9.55	26.01	3.57	6.70	12.46	1.80	1220	2.57	0.85	24.48	98.91
40	0.09	0.94	10.73	77.68	10.55	7.49	87.25	2.05	1722	263.32	7.61	27.25	56.15
41	0.09	0.77	15.00	109.14	7.47	11.49	57.31	3.08	1072	7.96	5.65	55.54	142.93
42	0.05	0.27	15.06	79.64	5.28	12.17	32.75	3.29	1030	0.73	2.20	57.25	124.65
43	0.04	0.13	7.67	10.10	3.83	5.49	7.57	1.47	1003	0.28	1.12	10.56	36.49
44	1.06	6.61	8.43	720.96	10.55	5.91	729.74	1.60	1123	1809.35	68.06	48.05	45.93
45	0.04	0.26	11.64	29.56	5.44	8.19	13.74	2.21	1005	1.29	1.98	23.51	131.38
46	0.06	0.78	10.60	48.22	6.35	7.74	77.97	2.08	1571	263.64	6.55	45.85	52.44
47	0.04	0.15	7.13	18.01	4.56	5.08	7.70	1.37	1754	0.88	0.74	16.66	31.27
48	0.10	1.77	10.78	96.26	9.21	7.53	204.69	2.07	2050	160.88	17.47	33.80	56.07
49	0.01	0.07	8.41	8.62	4.65	5.90	4.64	1.60	1273	0.53	0.42	20.24	41.40
50	0.01	0.14	8.20	21.44	4.72	5.82	9.36	1.59	1605	1.13	1.09	15.69	34.74

51	0.07	0.32	16.73	74.37	4.72	13.37	15.49	3.58	1543	1.48	1.61	42.65	179.10
53	0.11	0.61	18.32	115.72	7.17	15.01	105.05	4.06	1142	4.30	5.57	54.24	144.83
54	0.09	1.89	11.48	71.73	7.76	8.22	115.81	2.22	1991	232.04	18.75	34.35	58.20

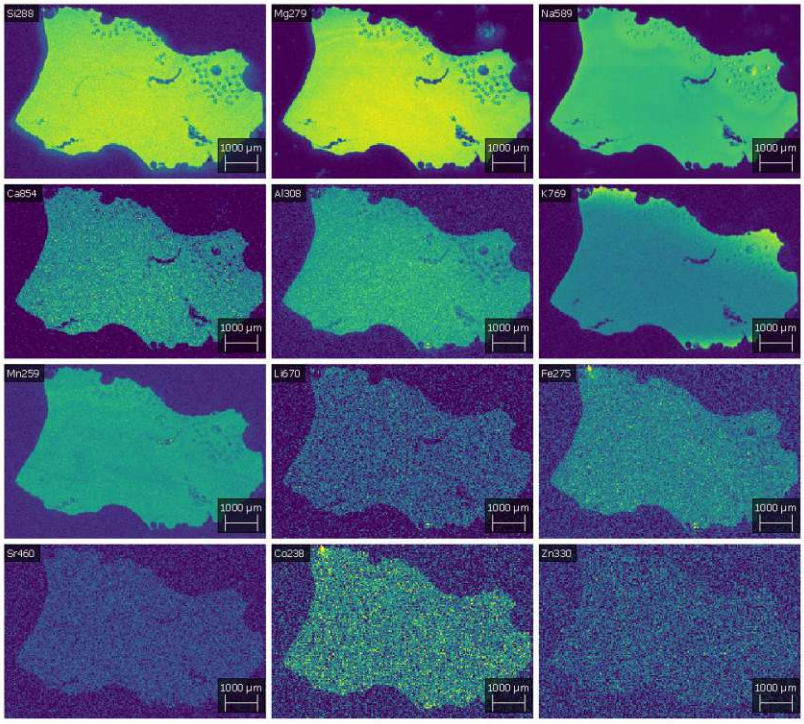

Figure 9.3: Imaging results Sample 40

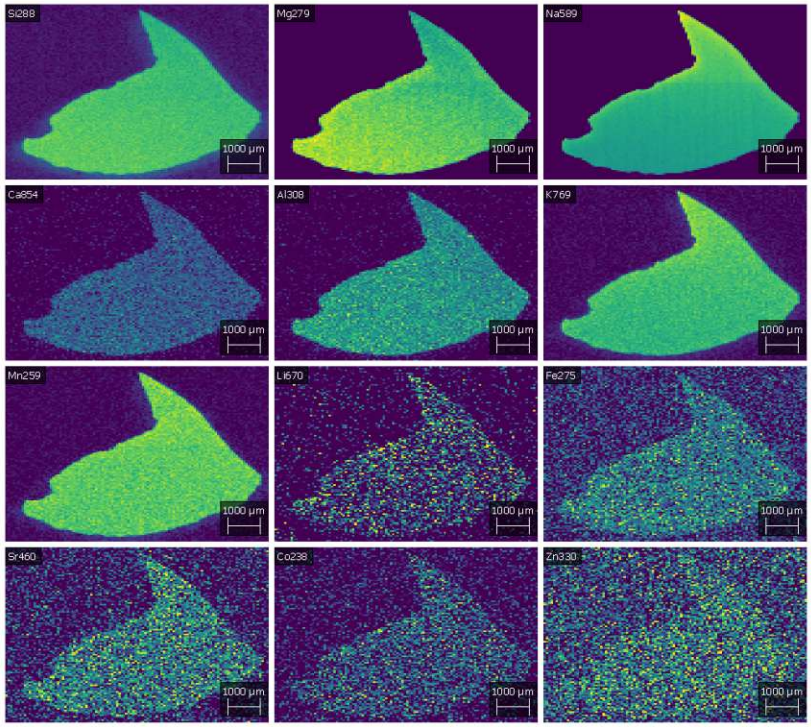

Figure 9.4: Imaging results Sample 25

Table 9.8: Mean compositions of samples assigned to different provenances with the SD

	without RM		with RM			novelty
Mean and SD [µg/g]	Egypt	Levant	Egypt	Egypt/Levant	Levant	Egypt
Na	130080	115198	122228	116342	120742	128457
	5336	7989	14069	5236	5552	10162
Mg	2595	2490	3176	3091	2644	2598
	479	538	306	174	475	627
Al	10432	10142	12367	11258	11540	10561
	1632	1187	940	1155	1314	2301
Si	325588	325884	322784	322482	330326	326226
	5668	5622	6843	6147	6121	6092
K	1996	2378	2726	2901	3000	1983
	228	372	231	256	383	505
Ti	1489	424	1411	621	527	1836
	1182	124	627	142	203	1216
Ba	879	257	327	379	344	289
	1356	29	79	57	45	164
Ca	48883	62328	56774	62199	63522	46272
	6164	4692	6972	4332	5808	5913
Fe	10736	5521	17648	8838	6368	11645
	7108	1819	4334	2776	1383	7475
Mn	6927	5374	7116	7994	5827	4265
	2598	2822	2624	689	1904	3570
Sr	486	582	616	737	629	421
	60	77	62	89	187	69
S	1360	1328	1252	1550	1445	1472
	370	435	320	288	560	383
Li	5	6	7	8	8	5
	1	2	1	2	3	1
Cu	35	25	637	88	457	214
	24	20	891	42	452	555
Zn	25	22	61	34	37	31
	10	9	26	7	13	17
Zr	92	41	95	55	46	108
	59	13	46	8	12	67
Cd	0	0	3	1	4	0
	0	0	3	0	4	0
Sn	2	4	28	12	43	3
	2	3	35	4	40	4
Sb	9	23	77	137	584	393
	18	34	114	90	603	1238
Pr	2	2	3	2	2	2
	1	0	1	0	0	1
Ce	10	9	13	10	9	11
	3	1	5	2	1	3
Nd	8	6	10	7	7	8
	2	1	5	1	1	3

Pb	29	35	1162	149	340	150
	45	36	1726	80	418	409